THE JOURNAL OF COMPARATIVE NEUROLOGY 494:7–35 (2006)

Columnar Projections from the Cholinergic Nucleus Isthmi to the Optic Tectum in Chicks (*Gallus gallus*): A Possible Substrate for Synchronizing Tectal Channels

YUAN WANG,[1] HARALD LUKSCH,[2] NICHOLAS C. BRECHA,[3] AND HARVEY J. KARTEN[1]*

[1]Department of Neurosciences, School of Medicine, University of California, San Diego, La Jolla, California 92093-0608

[2]Institute of Biology II, Rheinisch-Westfälische Technische Hochschule Aachen, 52074 Aachen, Germany

[3]Department of Neurobiology, School of Medicine, University of California, Los Angeles, Los Angeles, California 90095-1763

ABSTRACT

The cholinergic division of the avian nucleus isthmi, the homolog of the mammalian nucleus parabigeminalis, is composed of the pars parvocellularis (Ipc) and pars semilunaris (SLu). Ipc and SLu were studied with in vivo and in vitro tracing and intracellular filling methods. 1) Both nuclei have reciprocal homotopic connections with the ipsilateral optic tectum. The SLu connection is more diffuse than that of Ipc. 2) Tectal inputs to Ipc and SLu are Brn3a-immunoreactive neurons in the inner sublayer of layer 10. Tectal neurons projecting on Ipc possess "shepherd's crook" axons and radial dendritic fields in layers 2–13. 3) Neurons in the mid-portion of Ipc possess a columnar spiny dendritic field. SLu neurons have a large, nonoriented spiny dendritic field. 4) Ipc terminals form a cylindrical brush-like arborization (35–50 μm wide) in layers 2–10, with extremely dense boutons in layers 3–6, and a diffuse arborization in layers 11–13. SLu neurons terminate in a wider column (120–180 μm wide) lacking the dust-like boutonal features of Ipc and extend in layers 4c–13 with dense arborizations in layers 4c, 6, and 9–13. 5) Ipc and SLu contain specialized fast potassium ion channels. We propose that dense arborizations of Ipc axons may be directed to the distal dendritic bottlebrushes of motion detecting tectal ganglion cells (TGCs). They may provide synchronous activation of a group of adjacent bottlebrushes of different TGCs of the same type via their intralaminar processes, and cross channel activation of different types of TGCs within the same column of visual space. J. Comp. Neurol. 494:7–35, 2006.

Indexing terms: nucleus isthmi pars parvocellularis; nucleus isthmi pars semilunaris; nucleus parabigeminalis; tectal ganglion cell; motion detecting; timing

The isthmic complex in birds, consisting of the nucleus isthmi pars magnocellularis (Imc), pars parvocellularis (Ipc), and pars semilunaris (SLu, see Fig. 1), is reciprocally connected with the optic tectum (TeO). The avian isthmi and its homologous structure in amphibians and reptiles are postulated to participate in various visual

Grant sponsor: National Institute of Neurological Disorders and Stroke; Grant number: NS 24560-15 (to H.J.K.); Grant sponsor: National Institute of Mental Health (to H.J.K.); Grant number: NH 60975-07; Grant sponsor: Deutsche Forschungsgemeinschaft; Grant number: Lu 622 8-2 (to H.L.).

This article is dedicated to Yuan Wang's teacher, Dr. Shu-Rong Wang.

The first two authors contributed equally to this work.

*Correspondence to: Harvey J. Karten, Department of Neurosciences, School of Medicine, U.C. San Diego, 9500 Gilman Drive, La Jolla, CA 92093-0608. E-mail: hjkarten@ucsd.edu

Received 11 May 2005; Revised 10 June 2005; Accepted 15 August 2005

DOI 10.1002/cne.20821

Published online in Wiley InterScience (www.interscience.wiley.com).

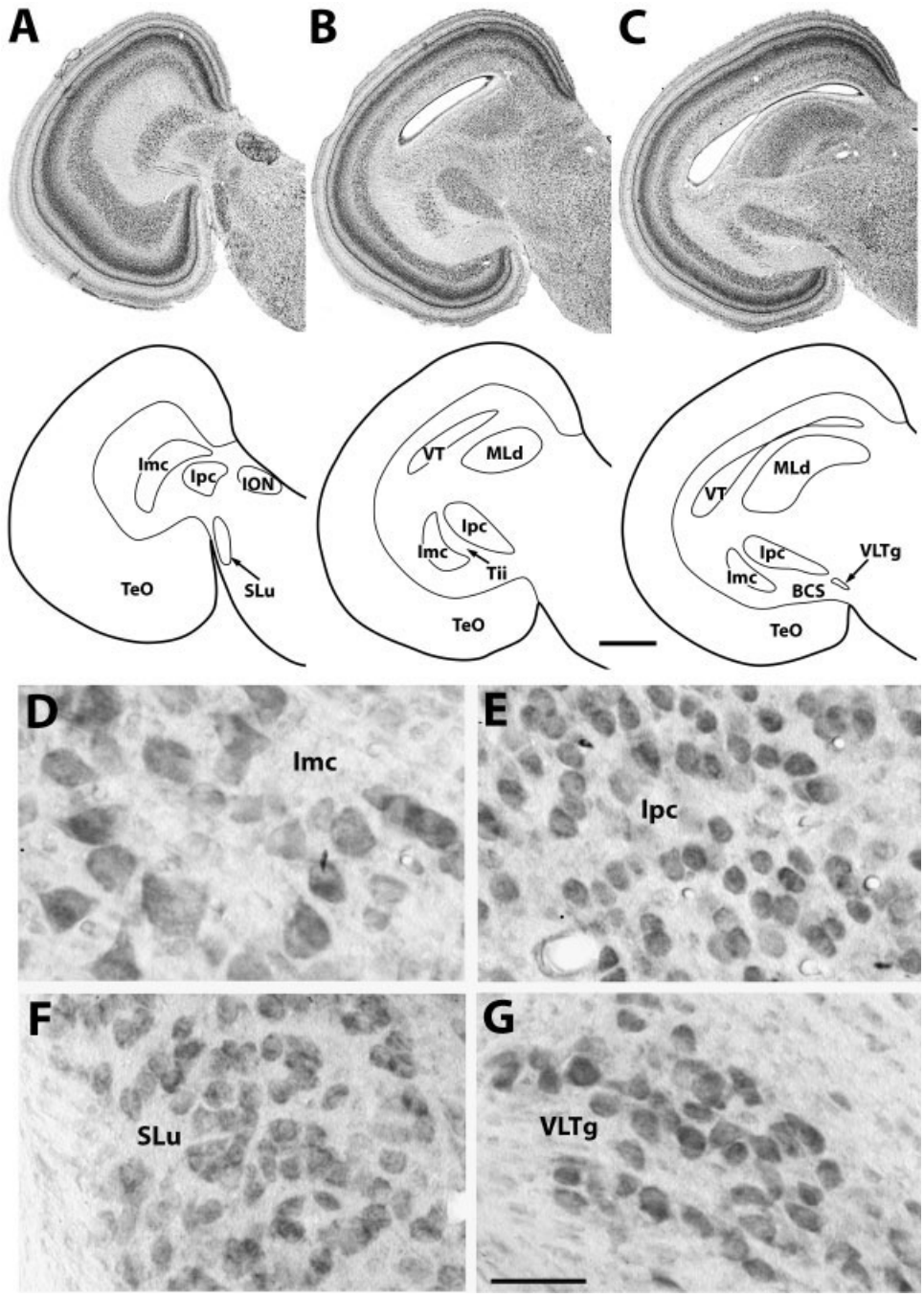

Fig. 1. Relative location and cytoarchitecture of isthmic nuclei in coronal Nissl-stained sections. **A–C:** Microphotographs and line drawings of the caudal (A) and intermediate (B,C) optic lobe. Note that SLu and the more rostrally located VLTg are not continuous. **D–G:** Nissl-stained neurons in Imc (D), Ipc (E), SLu (F), and VLTg (G). Imc, nucleus isthmi pars magnocellularis; Ipc, nucleus isthmi pars parvocellularis; SLu, nucleus isthmi pars semilunaris; VLTg, nucleus ventrolateralis tegmenti; TeO, optic tectum; ION, nucleus isthmo-opticus; Tii, tractus intraisthmicus; VT, ventriculus tecti mesencephali; MLd, nucleus mesencephalicus lateralis pars dorsalis; BCS, brachium colliculi superioris. Scale bars = 1 mm in B (applies to A–C); 50 μm in G (applies to D–G).

activities of the tectal system, such as stabilization of retinotectal terminals (frog: Gruberg et al., 1991), construction of center-surround interactions or "winner-take-all" networks (turtle: Sereno and Ulinski, 1987; Pigeon: Wang and Frost, 1991; Wang, 2003), generation of tectal fast oscillations (pigeon: Marín et al., 2005), and synchrony of parallel tectothalamic channels (chick: Wang et al., 2004).

Despite growing interest in these nuclei over the past 20 years, their connections and functional roles have been obscure. In a recent study (Wang et al., 2004), we described the organization and connections of the Imc. Imc contains GABAergic neurons and receives a coarse topographical projection from the radial neurons located in tectal layers 10–11. Neurons in Imc are grouped into two types on the basis of their differential projections: 1) *Imc-Is* neurons, which terminate extensively on the Ipc and SLu, and 2) *Imc-Te* neurons, which terminate on the deep tectal layers in a *heterotopic* manner, i.e., Imc neurons project diffusely on the TeO but not to the locus from which they receive input. The organization and connections of Imc may mediate its participation in a center-

surround interaction. A major mode of action of Imc, however, appears to occur consequent to its projections on Ipc and SLu. Thus, in order to understand the totality of operations of these nuclei, we need additional information regarding the organization and functions of Ipc and SLu.

The current article extends our analysis to the Ipc and SLu. Ipc and SLu, collectively, appear to be homologous to the nucleus parabigeminalis of mammals (Le Gros Clark, 1933; Diamond et al., 1992) and the nucleus isthmi of other nonmammalian vertebrates (see Wang, 2003). The avian Ipc and SLu lie adjacent to each other and share a number of prominent features. They both contain cholinergic neurons (Sorenson et al., 1989; Medina and Reiner, 1994) and maintain parallel and independent topographically organized reciprocal connections with the TeO (Hunt and Künzle, 1976; Hunt et al., 1977; Brecha, 1978; Güntürkün and Remy, 1990; Hellmann et al., 2001). These reciprocal connections are organized in a precisely homotopic manner, i.e., any single portion of the TeO is connected with a corresponding point in Ipc and in SLu (Brecha, 1978; Hellmann et al., 2001; Wang et al., 2004). They both receive a nontopographical input from the Imc (Wang et al., 2004). A major difference between the organization of Ipc and SLu is a thalamic/pretectal projection in pigeons arising from SLu but not from Ipc (Hellmann et al., 2001).

The almost identical pattern of the organization of Ipc and SLu within the isthmotectal circuitry appears paradoxical. Are they separate cell groups of distinct functional importance, or do they act as a unitary functional structure divided into two parts by passing fibers? Another mystery pertaining to this system is the functional role of the precisely homotopic reciprocal isthmotectal connections. What is the purpose of such a complex system of sending axons outside the TeO to a cell group, only to project back to the same location? In order to clarify these issues a detailed description of the cellular substrate of the interaction between the TeO and Ipc/SLu is required.

The detailed morphology and laminar distribution of the axonal terminals of Ipc/SLu neurons have not been adequately clarified, although the projection from the isthmic area on the TeO was first described in Golgi-stained materials by Pedro Ramón (cited in Ramón y Cajal, 1899, 1911) more than a century ago. "Fibers ending in a pinceau or brush-like arrangement form a very curious type of axonal arborization. The fibers themselves are the thickest in the optic lobe. … The branches generate a strange plexus with no counterpart anywhere in the central nervous system. … The unusual thickness of the parent fibers, the dendritic varicosity at the base of the ramification, and the extraordinary shape of the ramification itself were so surprising that we dared not consider it neuronal in nature" (Ramón y Cajal, 1911; translated by Swanson and Swanson, 1995:172–173).

However, Pedro Ramón erroneously attributed the origins of the unique "brush-like" axonal terminals to the Imc and not to the Ipc. Later investigators clearly ascribed the columnar axonal terminals to Ipc neurons by tract-tracing studies (Hunt et al., 1977; Sereno and Ulinski, 1987; Tömböl et al., 1995; Wang et al., 2004). Still, the description of the morphology and laminar distribution of Ipc terminals by different authors are not consistent with each other. Brush-like axonal terminals as described by Pedro Ramón extend from layer 10 externally to the margin of layer 1 in a relatively uniform density with a "dendritic varicosity at the base of the ramification" (fig. 139 in Ramón y Cajal, 1911). Hunt et al. (1977) suggested that the Ipc axons terminate most densely in layers 3 and 5, consistent with the characteristic laminar distribution in turtles (Sereno and Ulinski, 1987). Tömböl and colleagues (Tömböl et al., 1995; Tömböl and Németh, 1998) identified two types of columnar axonal terminals, a long one extending from layer 10 to 2 and a short one from 6 to 2, and suggested that only the short ones come from Ipc. In addition, the origin of brush-like axonal terminals from the Ipc has not been unambiguously confirmed at the single-cell level. The pattern of the axonal terminals of SLu neurons is even less well understood and their laminar distribution within the TeO has remained controversial. Anterograde tracing studies demonstrated a projection from SLu onto the intermediate and deep tectal layers (Brecha, 1978; Hunt and Brecha, 1984). However, retrograde tracing studies suggested that SLu neurons only terminate in the superficial tectal layers (Hellmann et al., 2001).

Whether tectal inputs on the Ipc and the SLu originate from the same tectal layers or cell types remains unknown. Bipolar neurons that lie within layers 10–11 of the TeO and project on Ipc have long been recognized (Ramón y Cajal, 1911; Woodson et al., 1991). These neurons are characterized by unusual "shepherd's crook" axons that arise from the apical dendrite, and then immediately make a 180° turn to leave the TeO through the deeper layers. Tectal neurons projecting on SLu have not been previously investigated, probably due to the difficulty in reaching this cell group located along the lateral margin of the tegmentum.

The current report, using multiple tract-tracing and intracellular filling techniques, provides a detailed description of the morphology and connections of Ipc/SLu neurons, with an emphasis on the cellular substrate of their reciprocal connections with the TeO. Distributions of cholinesterase, cytochrome oxidase, choline acetyltransferase, nicotinic acetylcholine receptors, and specific fast voltage-gated potassium channels Kv3.1 in the isthmotectal circuitry are also examined. Our results, together with the detailed knowledge of the morphology and connections of Imc (Wang et al., 2004) and tectal neurons (Luksch, 2003), provide the anatomical substrate of the isthmotectal interaction and allow a better assessment of the functions fulfilled by isthmic feedback loops.

MATERIALS AND METHODS

This study was performed on 98 White Leghorn chick hatchlings (*Gallus gallus*). All procedures used in this study were approved by University of California, San Diego Animal Care Committee, or the Animal Care Committee of RWTH Aachen and the Regierungspräsidium Köln, and conformed to the guidelines of the National Institutes of Health *Guide for the Care and Use of Laboratory Animals*.

Nissl, histochemical, and immunocytochemical staining

Six chicks of less than 5 days of age were anesthetized with a mixture of 40 mg/kg ketamine and 12 mg/kg xylazine and transcardially perfused with 0.9% saline followed by chilled 4% (or 2% for immunohistochemistry for nicotinic acetylcholine receptors) paraformaldehyde in phos-

phate buffer (PB; 0.1 M, 7.2–7.4 pH). The brains were removed from the skull, postfixed overnight in the paraformaldehyde solution, and then transferred to 30% sucrose in PB until they sank. Each brain was frozen, cut coronally or parasagittally at 30 μm on a freezing sliding microtome, and each section was collected in phosphate-buffered saline (PBS; 0.1 M, 7.2–7.4 pH). Sections from alternate series were stained for Nissl substance, histochemically for acetylcholinesterase (AChE; according to the procedure of Horton, 1984) and cytochrome oxidase (according to the procedure of Katz and Karten, 1983), or immunocytochemically for various substances described below.

Standard or fluorescent immunocytochemical methods were used to visualize the localization of choline acetyltransferase (ChAT), POU-domain transcription factor Brn3a, paired homeodomain factor Pax7, calbindin (CaBP), parvalbumin (PV), α7, α8, and β2 subunits of nicotinic acetylcholine receptors (nAChRs), and potassium channels Kv3.1. Briefly, sections were incubated with appropriate primary antibodies solution diluted in PBS (Anti-ChAT, 1:5000; Anti-Brn3a, 1:50; Anti-Pax7, 1:10; Anti-CaBP, 1:10,000; Anti-PV, 1:10,000; Anti-α7 nAChR, 1:500; Anti-α8 nAChR, 1:500; Anti-β2 nAChR, 1:500; Anti-Kv3.1b, 1:1,000) with 0.3% Triton X-100 overnight at 4°C, followed by biotinylated IgG antibodies (1:200; Vector Laboratories, Burlingame, CA) or secondary antibodies conjugated with fluorescent dyes (1:100; Jackson ImmunoResearch Laboratories, West Grove, PA) for 1 hour at room temperature.

Polyclonal anti-ChAT was kindly donated by Dr. Miles Epstein. The antibody was made in mouse against the protein of ChAT extracted from chick optic lobes (Johnson and Epstein, 1986). In Johnson and Epstein's study (1986), the specificity of the antiserum was evaluated in immunoblots. The immune serum "bound to a single band" of 64K molecular weight from the affinity-purified enzyme preparation, "identical to the single protein band observed in purified ChAT," and "stained immunoblots of the partially purified enzyme preparation."

Anti-Brn3a and anti-Pax7 antibodies were kindly donated by Dr. Eric Turner. Polyclonal anti-Brn3a antibody was generated in rabbits immunized with amino acids 130–210 of chick Brn-3.0 protein (Gerrero et al., 1993; Fedtsova and Turner, 1995). In Fedtsova and Turner's study (1995), the specificity of the Brn-3.0 antisera was tested by Western blotting, which "revealed a major band" of 43K molecular weight, "consistent with the predicted size of the Brn-3.0 cDNA open reading frame." Monoclonal anti-Pax7 was produced in mouse against chick Pax7, amino acids 352–523, in Dr. Atsushi Kawakami's laboratory (Nagoya University, Japan). The specificity of the antibody was not reported; however, the antibody "does not react with Pax3" based on unpublished data of Dr. Kawakami cited in Ericson et al. (1996).

Monoclonal anti-calbindin-D-28K and anti-parvalbumin were purchased from Sigma (St. Louis, MO; Lot #082K4879 and Lot #017H4821). Both antisera were made in mouse. Calbindin-D-28K purified from bovine kidney and parvalbumin from carp muscle were used as the immunogens, respectively. Anti-calbindin-D-28K reacts specifically with calbindin-D-28K in different tissues and cell populations. Anti-parvalbumin reacts specifically with parvalbumin of cultured nerve cells and tissue, and specifically stains the ^{45}Ca-binding spot of parvalbumin (12K molecular weight) by immunobinding.

Localization of α7, α8, and β2 nAChR were identified by means of monoclonal antibodies 306, 305, and 270, respectively, kindly donated by Dr. Jon Lindstrom. The 305 and 270 antisera were produced in mouse and 306 antiserum in rat, using affinity-purified α8, β2, and α7 immunogen from chick brain (Schoepfer et al., 1990, Whiting et al., 1990). Western blot analysis showed that antibodies 306 and 305 bound, respectively, α-bungarotoxin binding proteins α1 and α2 subtypes of native chicken tissue (Schoepfer et al., 1990). Subunit specificity of the antibody 270 was determined by Western blot analysis in Whiting et al. (1990), which revealed a major band of 49K molecular weight.

Polyclonal anti-potassium channel Kv3.1b made in rabbit was purchased from Alomone Laboratory (Jerusalem, Israel, #APC-014). The immunogen is a synthetic peptide corresponding to amino acids 567–585 of rat Kv3.1b. Western blot analysis showed that the antibody "specifically recognized the same 92 kDa protein bands in both rat and chicken synaptosomal preparations" (Parameshwaran et al., 2001).

Immunohistochemistry for these antibodies revealed identical patterns of morphology and distribution of staining in the chick brain as in previously published data (Anti-ChAT: Johnson and Epstein, 1986; Anti-Brn3a and Anti-Pax7: Fedtsova and Turner, 2001; Anti-CaBP and Anti-PV: Pfeiffer and Britto, 1997; Anti-α7, α8, and β2 nAChR: Britto et al., 1992; Anti-Kv3.1b: Lu et al., 2004).

For standard immunocytochemical staining, sections were then incubated in avidin-biotin-peroxidase complex solution (ABC Elite kit; Vector Laboratories, Burlingame, CA) diluted 1:100 in PBS with 0.3% Triton X-100 for 1 hour at room temperature. Sections were incubated for 3–5 minutes in 0.025% 3-3′-diaminobenzidine (DAB; Sigma) with 0.01% hydrogen peroxide in PB. Sections were mounted on gelatin-coated slides and stained with 0.05% osmium tetroxide for 30 seconds. Sections were then dehydrated, cleared, and coverslipped with Permount (Fisher Scientific, Pittsburgh, PA). For fluorescent immunocytochemical staining, sections were washed in PBS, mounted, and coverslipped with glycerin in carbonate buffer.

In vivo CTB and PHA-L injections

Cholera toxin B-subunit (CTB) was used in vivo as both an anterograde and a retrograde tracer to examine the general pattern of the reciprocal connections between the TeO and Ipc/SLu. CTB was injected into Ipc in five animals, SLu in seven animals, and different portions of the TeO in 12 animals, according to the procedure described in our previous study (Wang et al., 2004). Briefly, animals were anesthetized using a mixture of ketamine and xylazine, placed in a stereotaxic head holder, the skull exposed, and a hole made above the injection site. A solution of 1% CTB (List Laboratories, Campbell, CA) in PB was injected through a glass micropipette using a pressure device (PicoSpritzer II; General Valve, Fairfield, NJ). In six other animals, *Phaseolus vulgaris* leucoagglutinin (PHA-L; Vector Laboratories) was placed into Ipc (two cases) or SLu (four cases) as an anterograde tracer to further examine the terminal pattern of Ipc and SLu axons. A 2.5% solution of PHA-L was injected iontophoretically by means of glass micropipettes whose tip diameter

varied from 2–10 μm. The parameters of iontophoretic injection were a constant positive current of 2–10 μA for 10 minutes to deposit a small amount of tracer.

After CTB or PHA-L injections, the micropipette was withdrawn from the brain and the wound was closed. After a survival time of 3–5 days animals were anesthetized with an overdose of anesthesia and transcardially perfused with 0.9% saline followed by chilled 4% paraformaldehyde. The brain was removed from the skull, postfixed overnight in the paraformaldehyde solution, and then transferred to 30% sucrose until they sank. Each brain was frozen and cut coronally at 30 μm on a freezing sliding microtome. Alternating series of sections were collected and stained for standard or fluorescent immunocytochemistry for CTB or PHA-L, Giemsa, and Nissl, respectively. The primary antibodies against CTB and PHA-L were purchased from List laboratories (CTB: made in goat, #703, 1:12,000; PHA-L: made in rabbit, #Q0205, 1:1000).

In vitro BDA and biocytin deposits and intracellular filling

Fifty-two chicks were anesthetized as described above and then decapitated. The brains were quickly removed from the skull, placed in a dish of chilled, oxygenated, and sucrose-substituted artificial cerebrospinal fluid (ACSF; 240 mM sucrose, 3 mM KCL, 3 mM $MgCL_2$, 23 mM $NaHCO_3$, 1.2 mM NaH_2PO_4, 11 mM D-glucose). The midbrain was blocked and sectioned at 500–1000 μm on a Vibroslice (Campden Vibroslice; World Precision Instruments, Sarasota, FL) in appropriate planes. Slices were collected and submerged in a collecting chamber containing ACSF (119 mM NaCL, 2.5 mM KCL, 1.3 mM Mg_2SO_4, 1.0 mM NaH_2PO_4, 26.2 mM $NaHCO_3$, 11 mM D-glucose, 2.5 mM $CaCL_2$) at room temperature and continuously oxygenated with carbogen (95% O_2, 5% CO_2).

Procedures used for depositing tracers into a nucleus and for intracellularly filling individual neurons have been described in detail in our previous study (Wang et al., 2004). Briefly, tracer was deposited into Ipc or SLu by inserting a metal needle into the tissue, whose tip was covered with crystals of either biotinylated dextran amine (BDA, 10,000 molecular weight, Molecular Probes, Eugene, OR), BDA conjugated rhodamine (10,000 molecular weight, Molecular Probes), or biocytin (Sigma). Intracellular filling was done in different slices which were transferred to a chamber (Model RC-27L Large Bath Chamber, Warner Instrument, Hamden, CT) perfused continuously with oxygenated ACSF at room temperature. A recording electrode (100–300 MΩ) filled with 4% biocytin (Sigma) in 0.3 M KAc (7.2–7.8 pH) was positioned over Ipc or SLu and advanced through the tissue. Cell penetration was indicated by a sudden negative voltage drop and cell discharges. Biocytin was iontophoresed into the neuron with 2–3 nA of positive current for 2–3 minutes. Only one cell was filled in a single slice.

Slices were kept in oxygenated ACSF for 6 hours following tracer deposit, or 15–60 minutes following intracellular filling. All slices were subsequently fixed by immersion in 4% paraformaldehyde in PB overnight. Sections injected with BDA conjugated rhodamine were washed in PBS, mounted, and coverslipped with glycerin in carbonate buffer. Other sections were transferred to 30% sucrose in PB until they sank. Each slice was frozen and resectioned at 80 μm on the freezing sliding microtome. Sections were collected in PBS, kept for 10 minutes in 0.6% hydrogen peroxide in methanol to block endogenous peroxidase activity, and washed again in PBS. Sections were then incubated in ABC complex solution at 4°C overnight. The reaction product was visualized with DAB. Counterstaining was avoided so as to not obscure fine cellular processes.

Imaging and cell reconstruction

Digital images of selected sections and cells were captured with a Nikon D100 digital camera mounted on a Nikon photomicroscope (Nikon, Tokyo, Japan), a Phase One digital studio camera system (Phase One A/S Denmark, Frederiksberg, Denmark), or an Olympus FV 300 confocal microscope. Image contrast adjustments and photomontages were performed using Adobe PhotoShop (Adobe Systems, Mountain View, CA). Detailed morphology of individual cells was reconstructed with a camera lucida on a Zeiss WL microscope (Carl Zeiss, Thornwood, NY). Measurements of dendritic field dimensions of individual cells were based on the cell reconstructions. Measurements of other cellular structures, such as soma size, dendritic and axonal caliber, and dimensions of injection sites and transportation zones, were done on calibrated images captured with a BW CCD camera, using the public domain NIH Image program. No corrections were made for tissue shrinkage.

RESULTS

Topography of the tecto-isthmic connections

In vivo CTB injections into the TeO confirmed the homotopic reciprocal connections between the TeO and both Ipc and SLu. In all cases the injection spread to both superficial and deep layers of the TeO and covered 1/100 to 1/20 area of the tectal surface. Within both Ipc and SLu, labeled terminals and neurons overlapped and were organized in columns perpendicular to the long axis of the nuclei (Fig. 2A,B). These columns were topographically distributed within the Ipc and SLu in direct relationship to the location of the injections (Fig. 2D). Injections into the caudal (cases a and b in Fig. 2D), intermediate (cases c and d in Fig. 2D), or rostral (case e in Fig. 2D) portions of the TeO labeled terminals and neurons in the caudal, intermediate, or rostral portions of Ipc and SLu, respectively. Injections into the dorsal (cases b and c in Fig. 2D) or ventral (cases a and e in Fig. 2D) portions of the TeO labeled terminals and neurons in the lateral or medial portions of Ipc and the dorsal or ventral portions of SLu, respectively.

Comparison of the extent of terminal labeling within Ipc and SLu further demonstrated that tectal inputs on SLu are organized in a less clearly segregated manner than the TeO-Ipc projection. For a given injection into the TeO, tectal terminals occupied a larger percentage of area in SLu than in Ipc. We define the relative occupation (RO) as the width of the labeled terminal columns at its largest extent divided by the length of the long axis of the nucleus. A larger RO suggests a more diffuse and extensive tectal input than a smaller RO. In our preparations, the value of RO in Ipc is consistently smaller than that in SLu in all cases (Fig. 2C). In order to evaluate the extent of distinct tectal projection zones within Ipc and SLu, BDA was placed into two adjacent

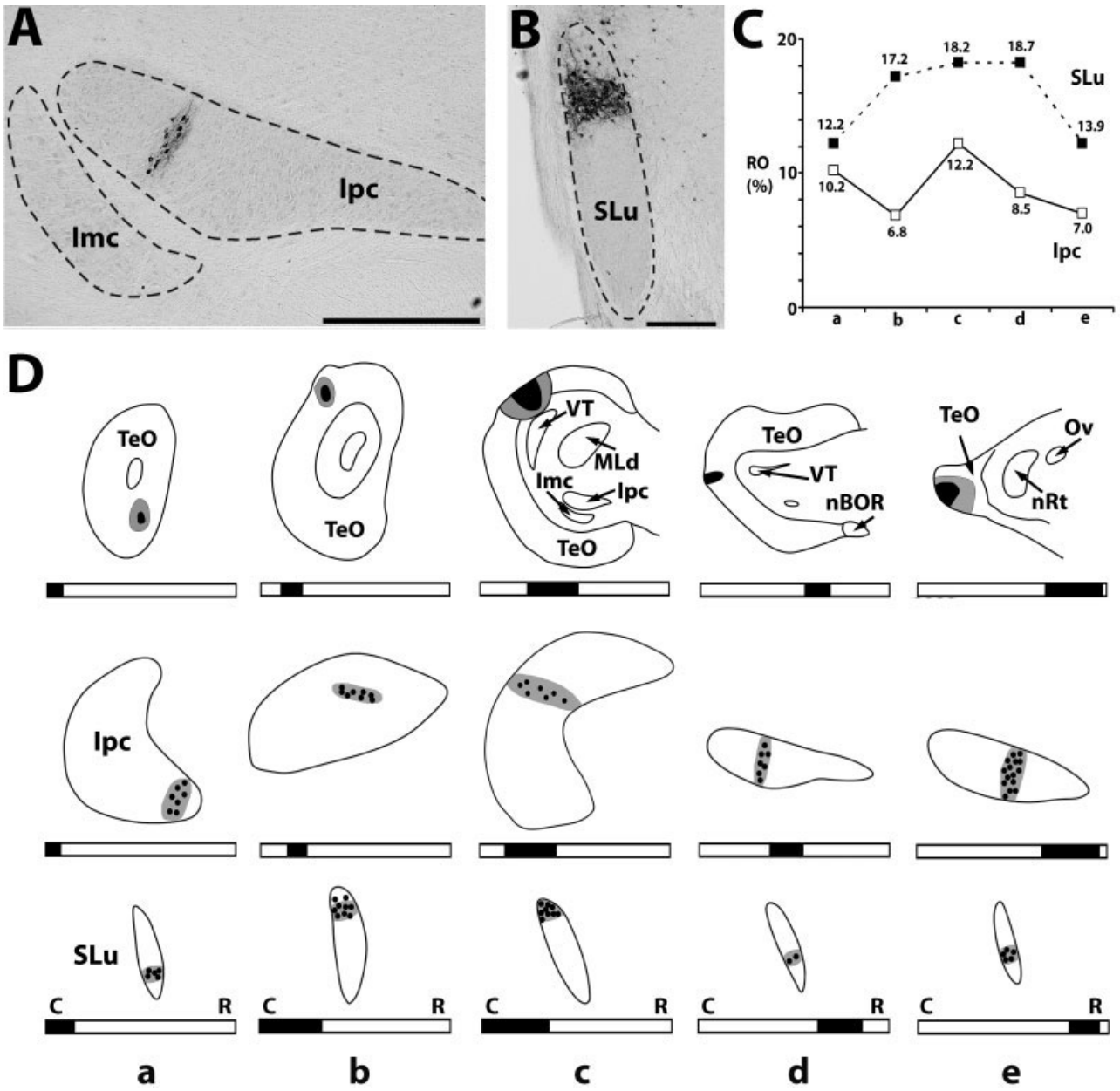

Fig. 2. Distribution of labeled neuropil and cells within Ipc and SLu in the coronal plane following in vivo CTB injections into the TeO. **A,B:** Columnar organization of labeled neuropil and cells within Ipc (A) and SLu (B). **C:** Relative occupation (RO) of tectal terminals in Ipc is smaller than that in SLu in five given cases (a–e) whose injection sites are charted in D. **D:** Line drawings illustrating the distribution of CTB labeling within Ipc and SLu in relationship to the injection sites in the TeO. The upper row illustrates the injection sites in the TeO. Black and gray areas represent the primary and peripheral zones of the injections, respectively. The middle and bottom rows illustrate the labeling patterns in Ipc and SLu, respectively. Gray shading and black dots indicate labeled neuropil and cells, respectively. Note that the labeled neuropil contains both anterogradely labeled tectal terminals and the dendrites of retrogradely labeled cells, which could not be differentiated from each other in CTB-labeled sections. For each drawing, up is dorsal and right is medial. The caudorostral level of each drawing is indicated by the underlying column. nBOR, nucleus of the basal optic root; nRt, nucleus rotundus; Ov, nucleus ovoidalis. Other abbreviations, see Figure 1. Scale bars = 500 μm in A; 200 μm in B.

locations of the TeO at the same caudorostral level, with one ventral to the other (Fig. 3A). The distance between the centers of these two injections was 450 μm. Two parallel terminal columns were labeled in Ipc, each about 80 μm in width with a 50-μm-wide label-sparse zone between them (Fig. 3B). In SLu, labeled terminals formed a single 150-μm-wide zone (Fig. 3C). This observation suggests that tectal terminals arising from these two injection sites were distributed in more obviously restricted and separate zones in Ipc, whereas the projections on SLu demonstrated greater overlap. However, this may merely reflect the more compact nature of

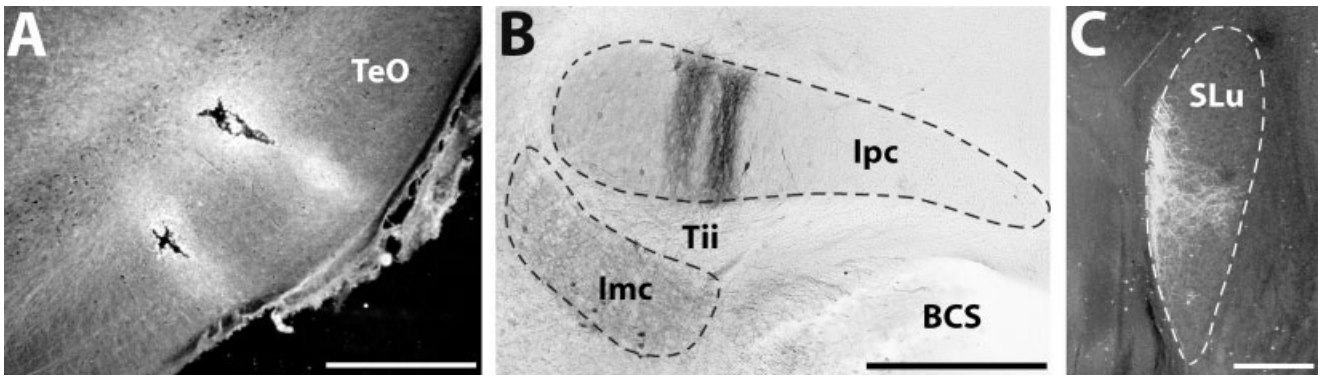

Fig. 3. Distribution of labeled axonal terminals within Ipc and SLu in the coronal plane following deposits of BDA in two adjacent locations of the lateral TeO. **A:** Deposit sites in the TeO. **B:** Two separate labeled columns of anterograde terminals in Ipc. **C:** One continuous labeled zone in SLu. Scale bars = 500 μm in A,B; 200 μm in C.

SLu, and smaller injections sites in the TeO may reveal a similar isolated topographical projection on SLu.

Tectal neurons projecting on Ipc and SLu

The TeO is a highly laminated structure and contains 15 alternating cell and fiber layers according to the nomenclature of Ramón y Cajal (1911). Some of these layers exhibit a sublayered organization. Of specific interest for the current study, layer 10 can readily be subdivided into layer 10a and 10b, the outer and the inner sublayers of layer 10, based on the variation of cell density and alignment, and the relative distribution of Pax7 vs. Brn3a labeled neurons. Within layer 10, Pax7-immunoreactive neurons are mostly situated in layer 10a, while layer 10b contains mostly Brn3a-immunoreactive neurons (see Fig. 6C,D).

TeO-Ipc neurons. In vivo CTB injections into Ipc demonstrated the laminar distribution of tectal neurons projecting on Ipc. Figure 4 illustrates an injection into the dorsal portion of Ipc, as well as the capsule dorsal to Ipc. Imc contained darkly labeled neurons throughout the nucleus, consistent with the extensive projection from Imc on Ipc (Wang et al., 2004). Within the TeO, most retrogradely labeled neurons were located in a restricted lateral portion of the TeO in layers 10–11, with the highest density in layer 10b. Other labeled cell populations included scattered neurons in layers 9, 12, 13, and 14 throughout a large portion of the TeO. As the TeO-Ipc projection is precisely topographical, those neurons may be labeled by tracer leakage into the capsule or cell groups located dorsally to Ipc. This assumption is supported by precise deposits of BDA into Ipc using slice preparations.

As in vivo injection of CTB usually produces a large diffuse deposit and CTB-labeled structures do not consistently provide sufficient details of their morphology, we further investigated the morphology of the TeO-Ipc neurons by depositing BDA or biocytin into Ipc in slice preparations. This technique has several advantages: 1) a relatively restricted injection could be achieved in slice preparations under direct visual control; 2) BDA and biocytin injection results in less diffusion at the injection site, with clearer definition of the immediately adjacent neurons; and 3) BDA and biocytin provide a clearer image of distant retrogradely labeled neurons, often filling the most distal terminals and their spine-like processes (Veenman et al., 1992; Wouterlood and Jorritsma-Byham, 1993). A significant disadvantage, however, is the relative insensitivity of these tracers, compared to that of CTB. With relatively comparable sized injections, CTB is more likely to label greater numbers of neurons.

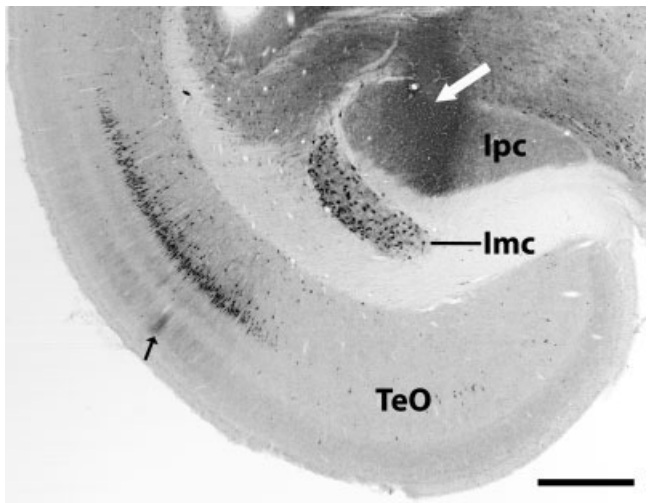

Fig. 4. Low-power view of the caudoventral optic lobe in the coronal plane following an in vivo CTB injection into Ipc. White arrow indicates the injection site. Labeled tectal neurons were mainly situated in layer 10b. Black arrow indicates a columnar axonal structure in layer 5. Scale bar = 500 μm.

In vitro BDA deposits into Ipc (Fig. 5A) confirmed the predominant location of retrogradely labeled neurons in layer 10b (Fig. 5B). Every single retrogradely labeled neuron in layer 10 was also immunoreactive for layer 10b marker Brn3a. These neurons had a radial dendritic field occupying a cylinder ~50–100 μm wide extending from layer 2 to 13 (Figs. 5C–F, 9). The basal dendrite extended deeply down to layer 13, with fine ramifications in layers 11, 12, and 13. The apical dendrite usually split into several parallel secondary branches in layers 9–10 (Figs. 5C,E, 9). Occasional neurons maintained a single thick

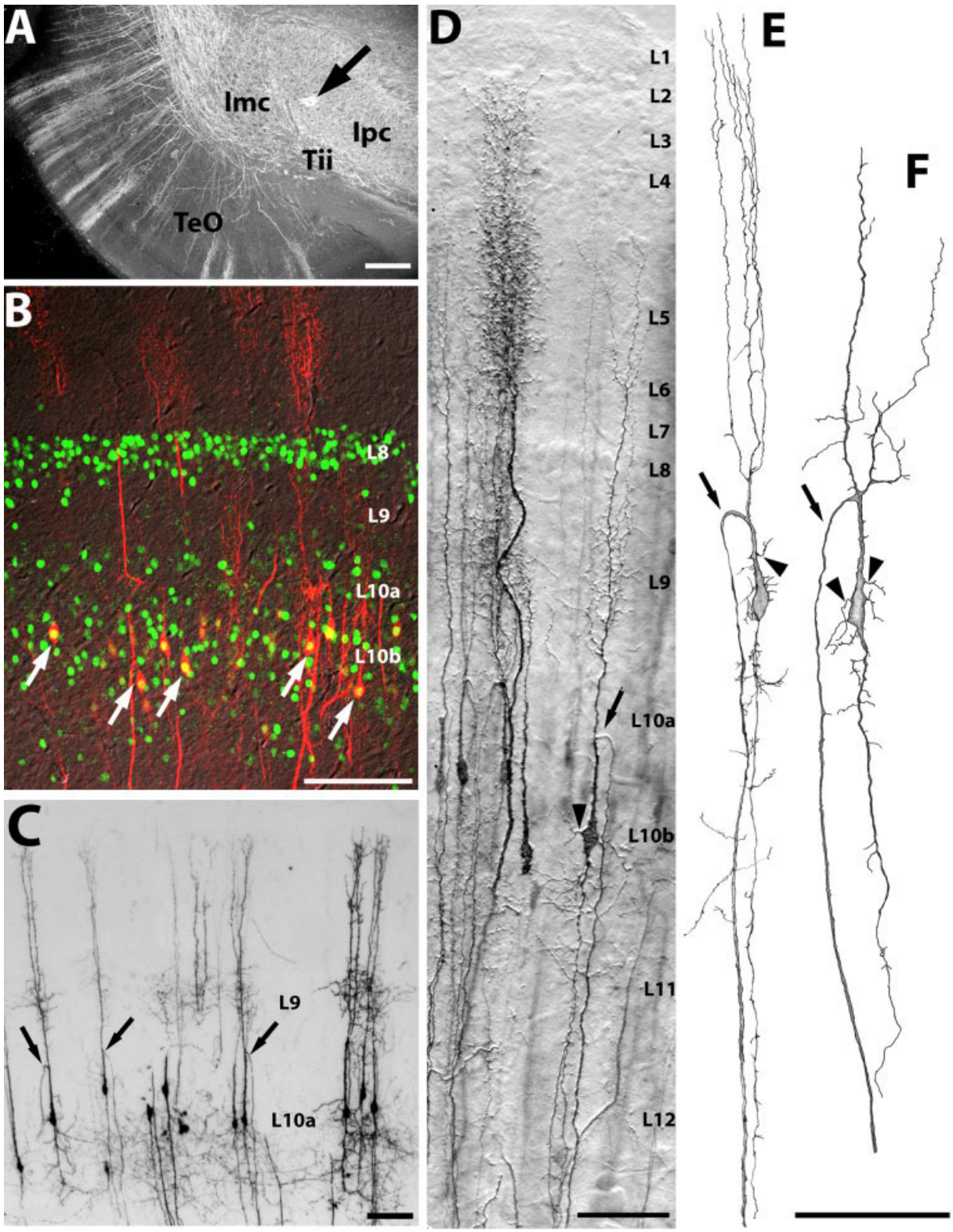

Fig. 5. In vitro BDA (A,B,D–F) or biocytin (C) deposits into Ipc in the horizontal plane. **A:** Low-power darkfield image of the injection site in Ipc (black arrow) and anterogradely labeled columnar structure terminals in the superficial tectal layers. **B:** Double labeling of immunocytochemistry for Brn3a (green) and BDA-labeled neurons (red). BDA-labeled neurons were mostly located in layer 10b and consistently double-labeled (yellow; white arrows) for Brn3a. **C:** Retrogradely labeled neurons in the TeO. **D:** Higher-power Nomarski-DIC image of a columnar axonal termination (left) and a radial tectal neuron (right). **E,F:** Camera lucida reconstructions of two radial tectal neurons. Small black arrows in C–F indicate the shepherd's crook axons. Arrowheads indicate the local dendrites emerging from the cell bodies and the trunk of the primary dendrites. Scale bars = 100 μm in A,E,F; 200 μm in B; 50 μm in C,D.

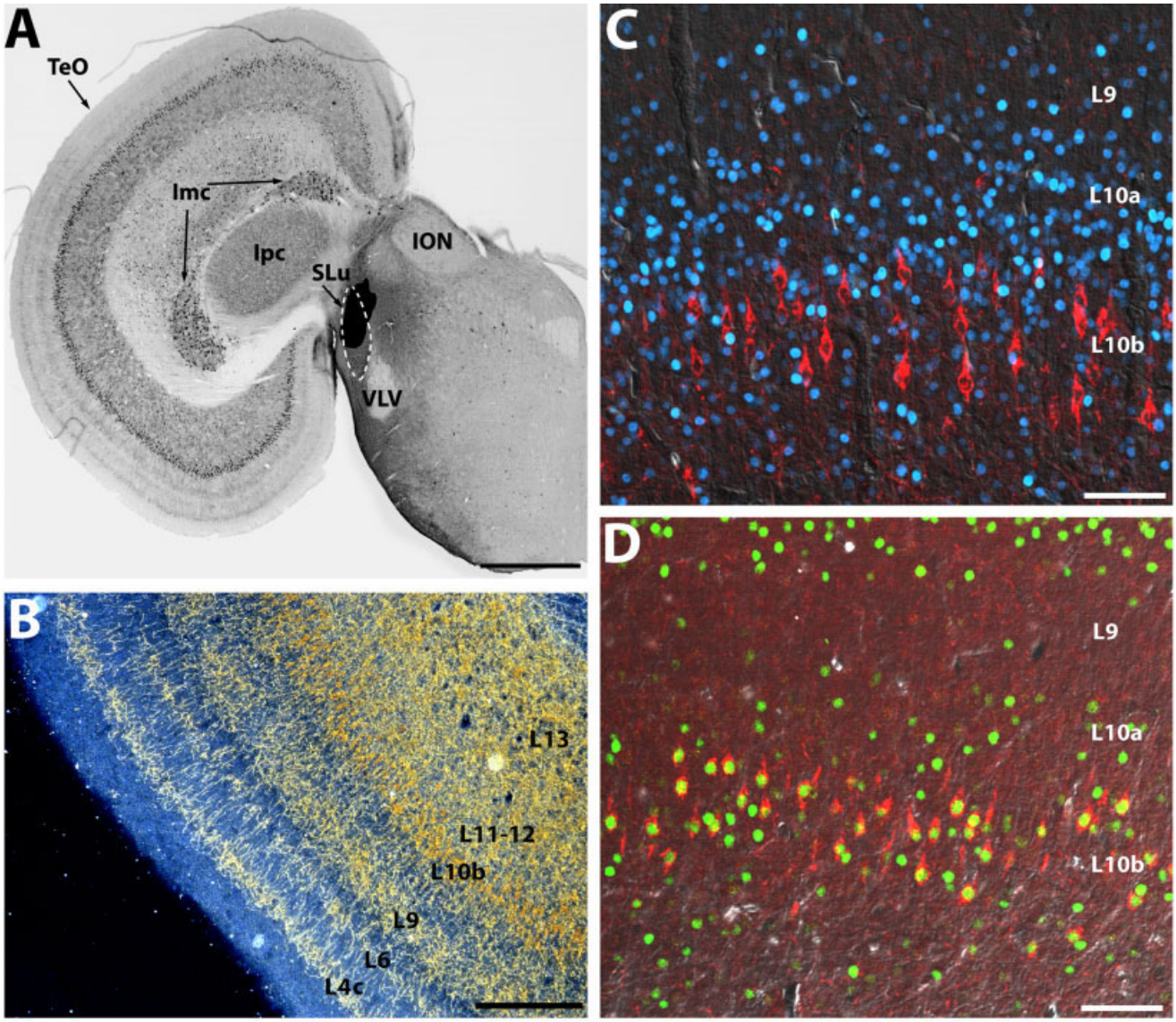

Fig. 6. In vivo CTB injection into SLu in the coronal plane. **A:** Low-power view of the caudal optic lobe illustrating the injection site and the general labeling pattern. Black shade indicates the center of the injection. **B:** Darkfield image of the ventrolateral TeO. Layers 4c, 6, 9, and 10b–13 contained heavily labeled neuropil. **C,D:** Double labeling of immunocytochemistry for CTB-labeled neurons (red) and Pax7 (blue, C) or Brn3a (green, D). CTB-labeled neurons were mostly located in layer 10b and exclusively double-labeled for Brn3a (yellow) but not for Pax7. Note that layer 10a contains more Pax7-immunoreactive cells and less Brn3a-immunoreactive cells than layer 10b. VLV, nucleus ventralis lemnisci lateralis. Other abbreviations, see Figure 1. Scale bars = 1 mm in A; 250 μm in B; 50 μm in C,D.

apical primary dendrite until layer 5 (Fig. 5D). Regardless of the arborization pattern, the apical dendrite extended up to layer 2 with the highest terminal density in layer 9. In addition, a few relatively thin dendritic branches issued from the soma or the basal trunk of the primary dendrites and terminated locally around the soma (arrowheads in Fig. 5D–F). The main axon arose from the primary apical dendritic trunk in layer 10 or along the border between layers 10 and 9, and turned immediately to course through deeper tectal layers in a classical "shepherd's crook" shape (arrows in Figs. 5C–F, 9), parallel to the basal dendrite with a distance up to 20 μm. The main axon issued some axonal collaterals within layers 11–13 (Fig. 5E,F). In addition to these radial neurons in layer 10, few neurons were labeled in layers 11 and 14. None of these neurons appeared to have shepherd's crook axons and radial dendritic fields.

TeO-SLu neurons. In vivo CTB injections into SLu revealed a similar laminar distribution of the TeO-SLu neurons as the TeO-Ipc neurons (Fig. 6). To avoid the leakage and damage of the TeO, Imc, and Ipc, the injection pipette was inserted from the opposite side of the brain through the cerebellum ventromedially across the midline to reach the SLu (Fig. 6A). The injection involved most parts of SLu and the capsule dorsomedial to SLu. The capsule lateral to SLu contained darkly labeled fibers that

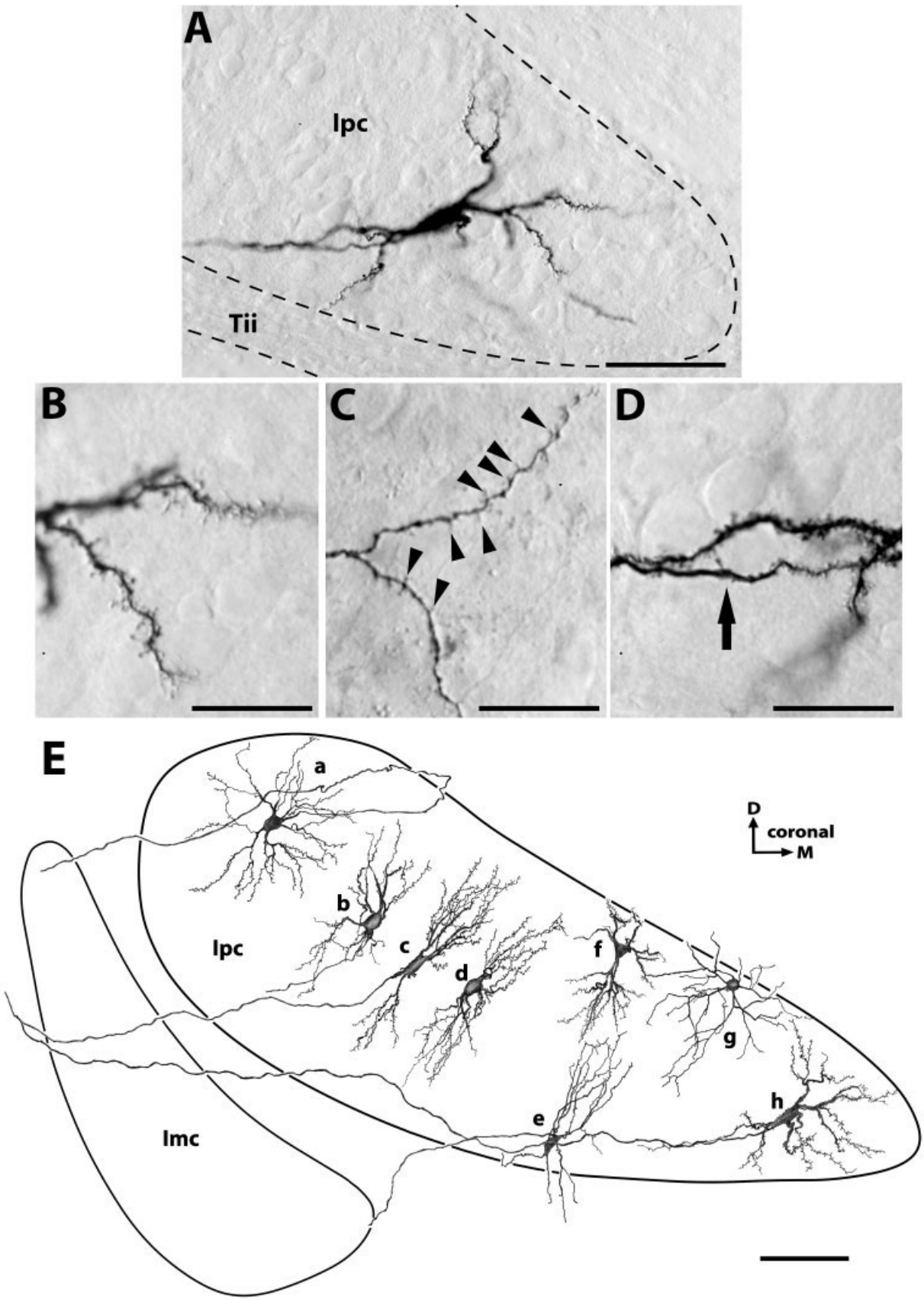

Fig. 7. Nomarski-DIC photomicrographs and camera lucida reconstructions of the somata and dendrites of intracellularly filled Ipc neurons in coronal slices. **A:** An Ipc neuron (cell h in E) gave off dendrites extending to the margins of the nucleus. Dashed lines indicate the borders of Ipc and Tii. **B:** Dense dendritic processes of a Type I Ipc neuron (cell h in E). **C:** Relatively sparse dendritic spines (arrowheads) of a Type II Ipc neuron (cell a in E). **D:** A spiny dendrite-like branch (right to the arrow) of a Type I Ipc neuron (cell h in E) turned into a smooth axon (left to the arrow). **E:** A montage drawing illustrates various dendritic patterns of Ipc neurons and their distribution within the nucleus. Scale bars = 100 μm in A,E; 40 μm in B–D.

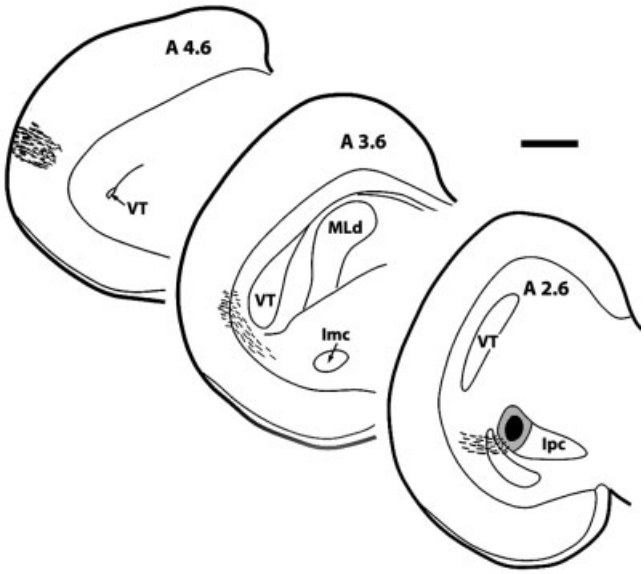

Fig. 8. Line drawings of the course of anterogradely labeled Ipc axons in the coronal plane after an in vivo PHA-L injection into the lateral Ipc. Scale bar = 1 mm.

extended ventrally along the lateral margin of the tegmentum. Imc contained darkly labeled neurons throughout the nucleus, consistent with the extensive projection from Imc on SLu (Wang et al., 2004), while Ipc did not contain any labeled neurons. Within the TeO, retrogradely labeled neurons were mainly found in layer 10b. Every single retrogradely labeled neuron in layer 10 was immunoreactive for layer 10b marker Brn3a (Fig. 6D), and was not immunoreactive for the layer 10a marker Pax7 (Fig. 6C). Apical and basal dendrites emerged from the ventral and dorsal poles of the cell body. However, their course and ramification could not be traced, and axons could not be detected unequivocally. In addition, a few scattered neurons were found in layers 14, 13, and 9. Unfortunately, we were unable to prepare slices that retain axons between the TeO and SLu. Morphology of the tectal neurons projecting on SLu could not be further examined in slice preparations.

Morphology of neurons in Ipc and SLu and their axonal terminations in the TeO

Figure 1A–C demonstrates the general cytoarchitecture of Ipc and SL in Nissl-stained sections. In contrast to the loosely packed large stellate cells in Imc (Fig. 1D), Ipc and SLu consist of closely packed round or oval cells, 18.0 ± 2.1 μm and 17.4 ± 2.3 μm, respectively, in diameter (Fig. 1E,F). Neurons in SLu form clusters of 3–8 cells. In addition to Imc, Ipc, and SLu, there is a fourth cell group located ventromedially to Ipc that may be mistakenly considered a rostral extension of SLu. However, this cell group is cytoarchitectually discontinuous from SLu (Fig. 1A–C) and contains slightly larger neurons, 19.4 ± 4.7 μm in diameter, than SLu (Fig. 1G). As this nucleus has not been named before, we call it the nucleus ventrolateralis tegmenti (VLTg) based on its location along the lateral margin of the tegmentum. No retrograde or anterograde labeling was detected in the VLTg following CTB injections into the TeO in our preparations.

Somatodendritic and local axonal morphology of Ipc neurons. Somatodendritic and local axonal morphology of Ipc neurons was investigated using intracellular fillings of individual neurons in 500-μm-thick slices in the coronal, parasagittal, and horizontal planes (Fig. 7). Somata of the filled neurons were mostly oval or round in shape. The long and short axes of the soma were, respectively, 19–29 and 8–18 μm long, with the long one usually oriented dorsoventrally. Four to six primary dendrites emerged from the dorsal and ventral portions of the soma and ramified two or three times within the nucleus. Most neurons in the middle of the nucleus formed a columnar dendritic field perpendicular to the long axis of the nucleus (cells b–f in Fig. 7E). These dendritic fields tended to cover the dorsoventral dimension of the nucleus so that the neurons located ventrally had longer dorsally oriented dendrites than the ventral ones (cell e in Fig. 7E), and vice versa (cell f in Fig. 7E). A single Ipc neuron occupied approximately a cylindrical volume of 70–150 μm width and 200–300 μm height. Neurons in the marginal part of the nucleus displayed various shapes of the dendritic fields and appeared to match the curving boundaries of the nucleus (Fig. 7A, cells a, g, and h in Fig. 7E).

Based on the density and distribution of dendritic spines and the origin of the axon, intracellularly filled Ipc neurons could be grouped into two types. Type I neurons carried a very high density of filiform spines, mushroom varicose, and/or hairlike processes in all orders of the dendrites and the soma (Fig. 7A,B, cells b, c, d, f, and h in Fig. 7E). Except for the most distal processes, the dendrites were thick, 2–5 μm in diameter, and labeled darkly. A comparable thick axon (2–4 μm in diameter) emerged either from a spiny primary dendrite or directly from the soma. For the latter, the first segment of the axon was always covered with a high density of spines and tapered with distance (Fig. 7D), resembling the basic features of a classical dendrite. At a distance of 10–40 μm from the soma, the dendrite-like structure became thicker and turned into a smooth axonal branch with a relatively stable caliber (arrow in Fig. 7D). Type I neurons were the major cell type in Ipc and distributed throughout the nucleus. In contrast, Type II neurons were much less frequently observed and mostly located in the marginal part of the nucleus (cells a, e, and g in Fig. 7E). They had relatively smooth soma and lower-order dendrites. Only the highest-order dendrites bore a moderate density of filiform spines (Fig. 7C). Dendrites of Type II neurons were 1–3 μm in diameter, relatively thinner than that of Type I neurons. A smooth primary axon was issued directly from the soma of Type II neurons. For both types of neurons the axon coursed laterally through Ipc and Imc without collateral within these two nuclei and penetrated into the tectal layer 14 where they usually passed out of the slices.

Distal axonal morphology of Ipc neurons within the TeO. The morphology of the distal axonal terminations of Ipc neurons within the TeO was examined with both in vivo and in vitro tracing studies and confirmed at the single cell level with intracellular filling of Ipc neurons.

In vivo CTB injections into Ipc labeled neuropil mainly in tectal layers 3, 5, and 9 (Fig. 4). Occasionally, a few dense columnar structures were found in layer 5 (black arrow). Some processes in layer 9 could be traced to retrogradely labeled somata in layer 10. As CTB was transported in both directions, anterogradely labeled axonal

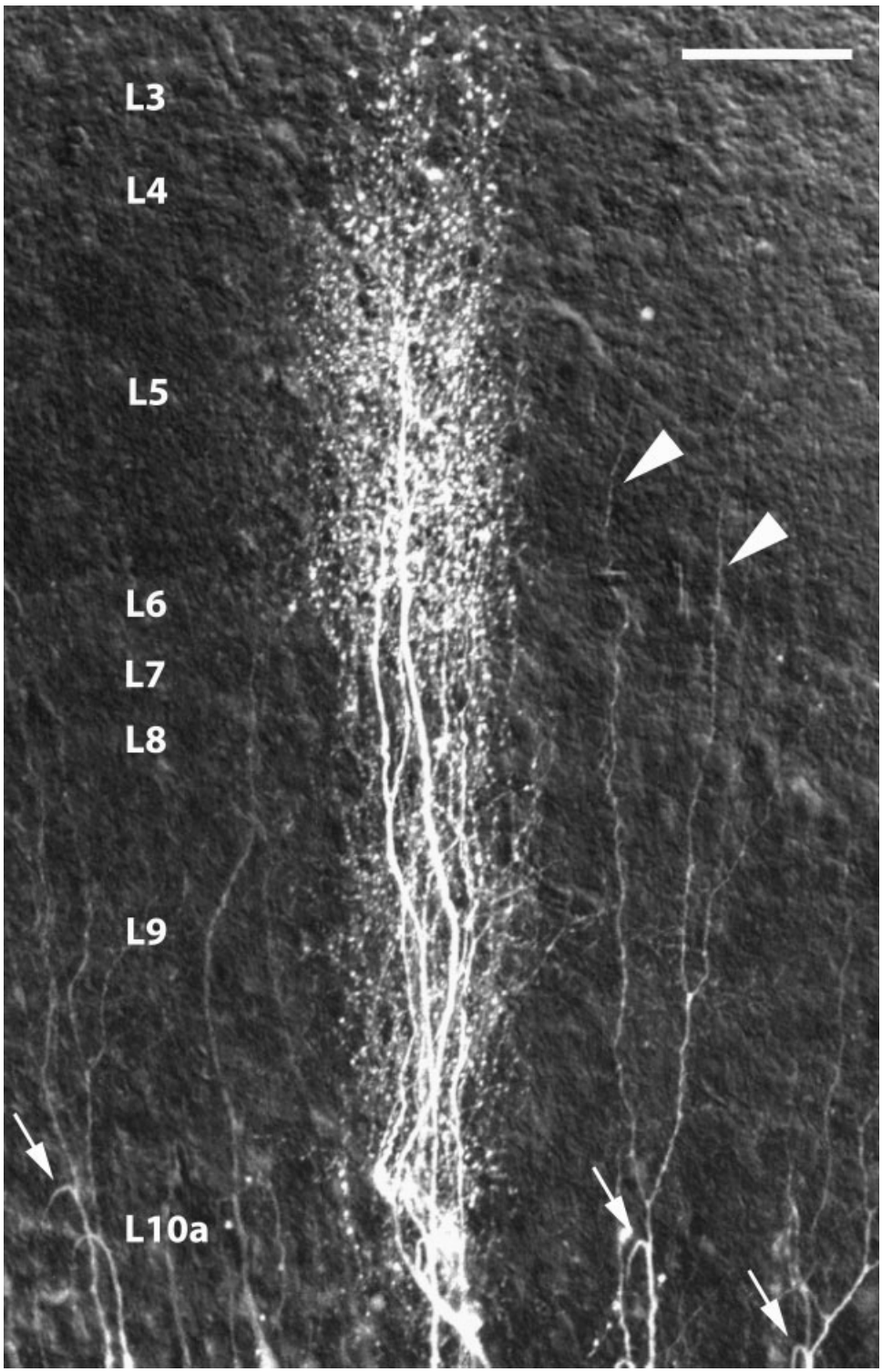

Fig. 9. Extended focus view of confocal microscopic Z-series of an individual Ipc brush-like ending in the horizontal plane following an in vitro injection of BDA conjugated with rhodamine into Ipc. Note the densest arborization in layer 5. Arrows indicate shepherd's crook axons of the tectal neurons labeled in the same slice. Arrowheads point out the long radial apical secondary dendrites of a tectal neuron. Note its dense fine dendritic ramification in layer 9. Scale bar = 50 μm.

terminals of Ipc neurons could not be reliably distinguished from retrogradely labeled tectal neurons and their dendrites. In contrast, PHA-L is mainly transported in an anterograde direction, and in comparison to CTB provides a denser and more uniform staining of single axons. After a restricted PHA-L injection into the lateral portion of Ipc, a bundle of thick axons left the injection site and extended rostrolaterally to the most distal terminals in the superficial tectal layers (Fig. 8). The trajectory of the Ipc axons was reconstructed from a series of coronal sections. The axons passed through Imc without any collateral arborizations, turned dorsally within layer 14 for a

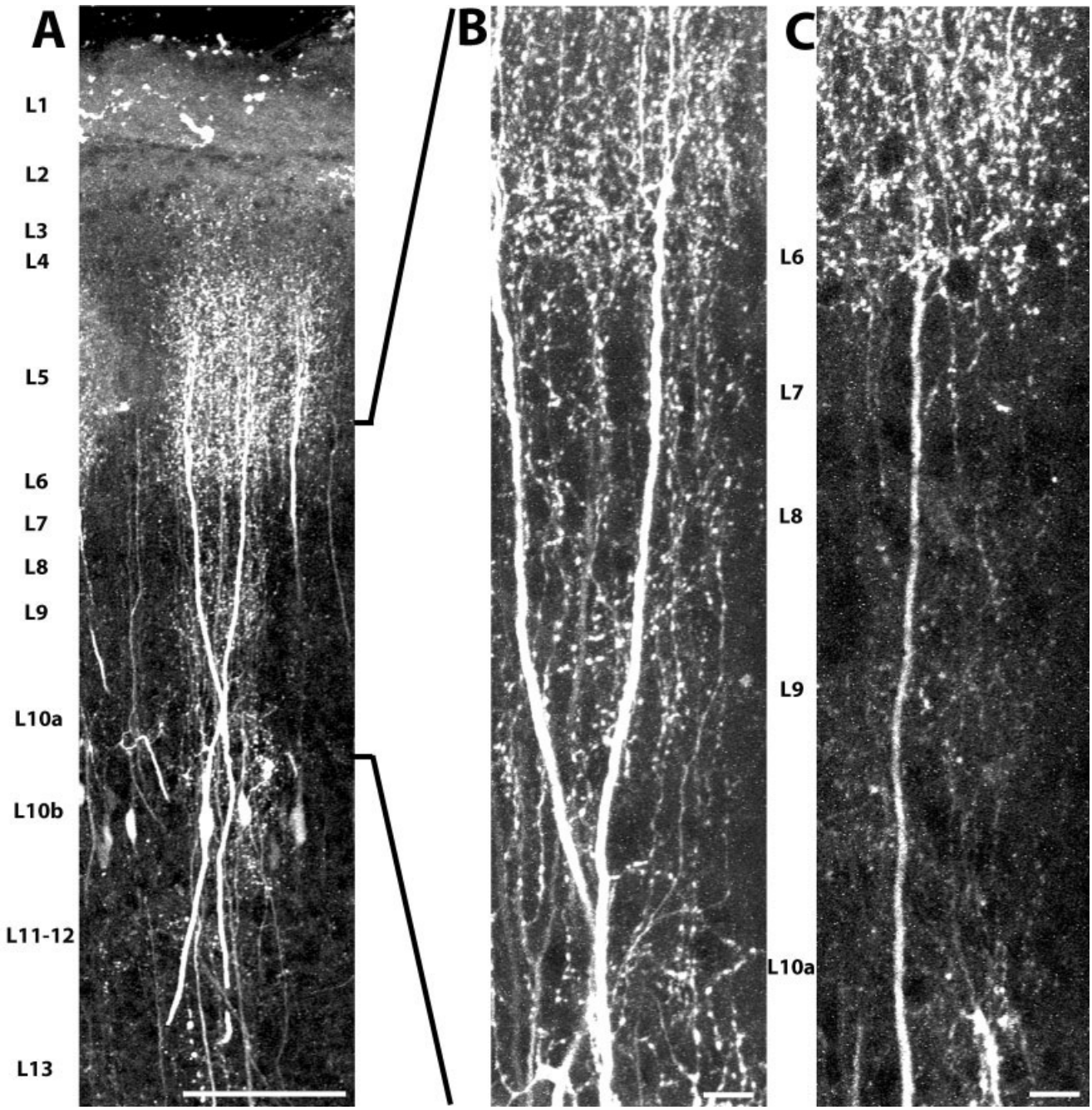

Fig. 10. Two variations of Ipc brush-like endings in the coronal plane following an in vitro injection of BDA conjugated with rhodamine into Ipc. **A:** Extended focus view of the complete confocal Z-series of the section. Note the densest arborization in layer 5. **B:** Extended focus view of the upper half of the section. Two thick axons issued many fine axonal branches in layer 10–7. **C:** Extended focus view of the lower half of the section. An individual axon remained smooth until layer 6, where it abruptly started to display dense terminations. Scale bars = 100 μm in A; 10 μm in B,C.

short distance, then abruptly turned laterally again and extended approximately perpendicular towards the surface of the TeO. These axons issued fine collaterals in layers 13–11, split into secondary branches in layer 10, and formed dense columnar terminations in layers 10–2.

Although in vivo PHA-L injections into Ipc suggested the columnar organization of the axonal terminations of Ipc neurons, the complete Ipc terminations across layers could not be visualized in the same sections because slices were made tangentially. To address this issue, we used 500-μm-thick brain slices with BDA deposits into Ipc and made repeated in vitro slice injections until we had samples cut in the radial plane of the TeO. This allowed us to demonstrate the full columnar extent of individual end-

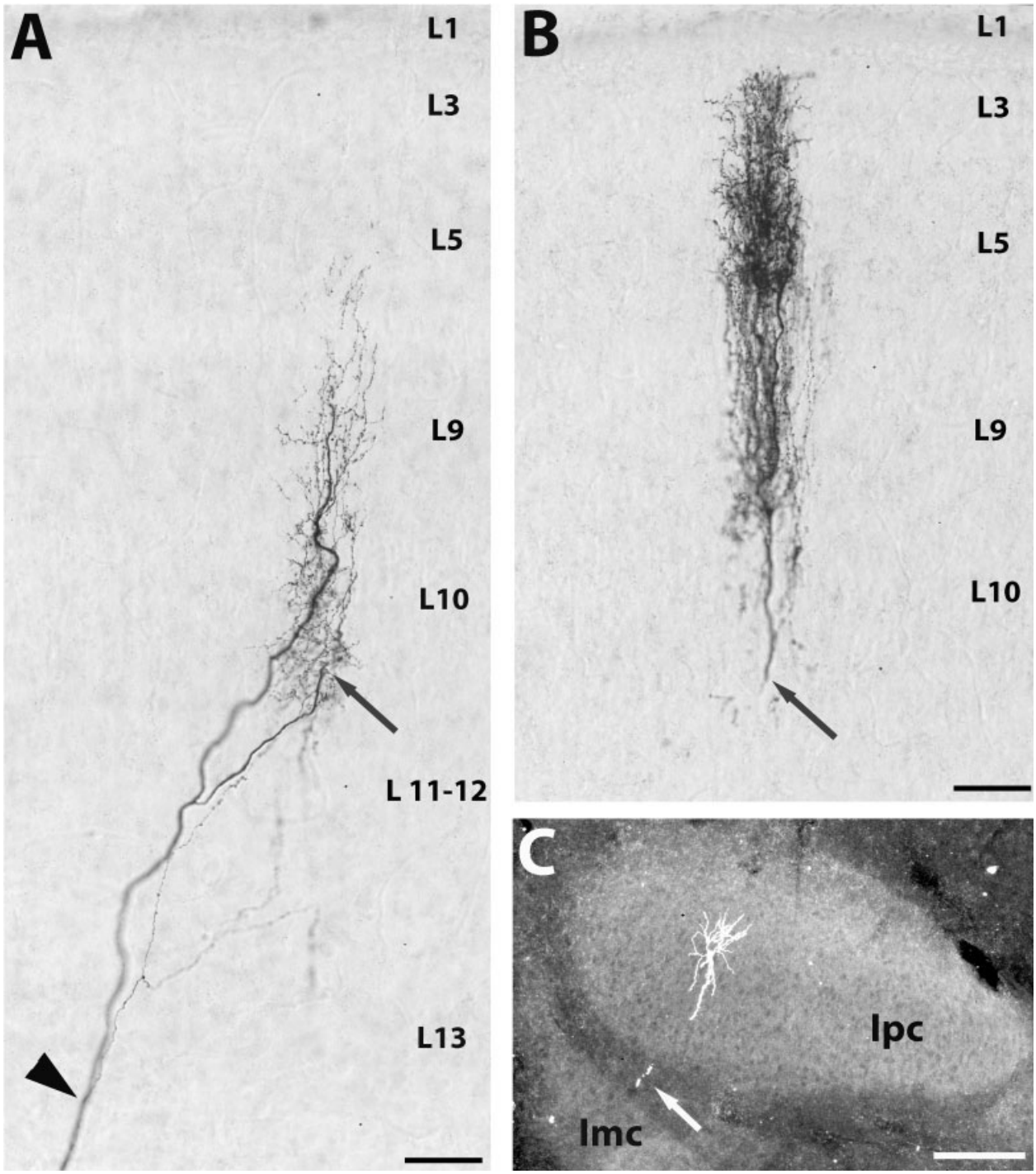

Fig. 11. Low-power view of an intracellularly filled Ipc neuron with its complete axonal arborizations. **A,B:** Axonal terminals of the Ipc neuron within the TeO in two adjacent sections from a single slice. A is at a more caudal level than B. Black arrows indicate the point where the Ipc axon was cut off during tissue resection. **C:** Darkfield image illustrating the location of the neuron in Ipc and a segment of the main axon within the Tii (white arrow). Scale bars = 50 μm in A,B; 200 μm in C.

ings, which were usually found in the caudal and ventrolateral portions of the TeO.

A large number of columnar axonal terminations were labeled in the TeO extending from layer 10 to 2 (Figs. 5A, 9, 10). Individual columnar endings were 35–50 μm wide and their terminal morphologies are consistent with the conspicuous dense vertical array of several thousand boutons in cylindrical *brush-like endings* described by Pedro Ramón (fig. 139 in Ramón y Cajal, 1911). Most of the axonal boutons were very small, ~0.7–1.5 μm in diameter,

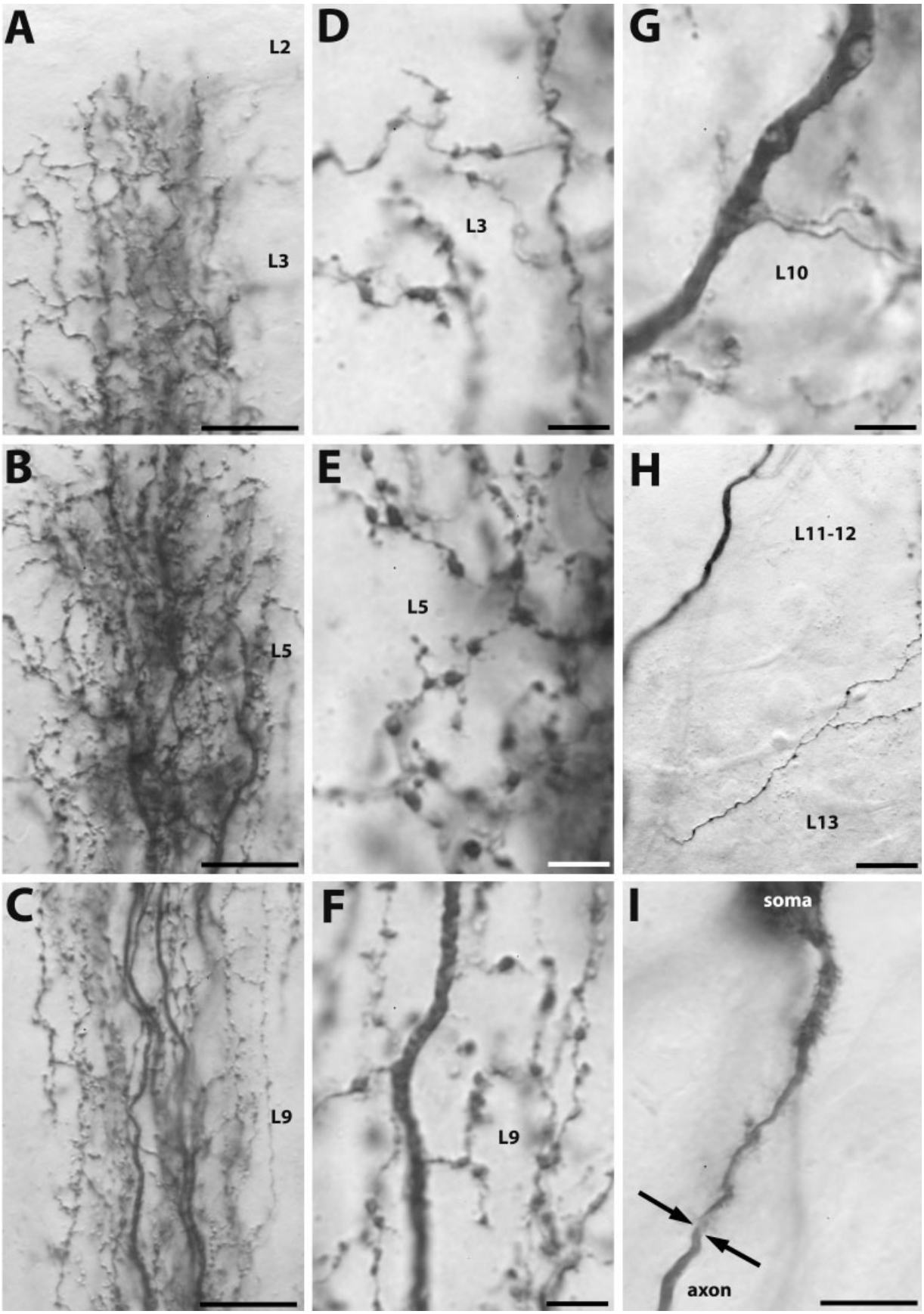

Fig. 12. Higher-power Nomarski-DIC view of the intracellularly filled Ipc neuron depicted in Figure 11. **A–C:** Distinct morphology of the brush-like endings in layers 3 (A), 5 (B), and 9 (C). **D–F:** Dense boutons in layers 3 (D), 5 (E), and 9 (F). **G:** A thick axonal stem gave off extremely thin branches. **H:** Fine axonal arborizations in layers 11–13 (bottom), in contrast to a thick axon stem (up). **I:** The origin of the primary axon (lower to the arrows) from a dendrite-like branch (upper to the arrows) which emerged directly from the soma. Scale bars = 20 μm in A–C,H; 5 μm in D–G; 10 μm in I.

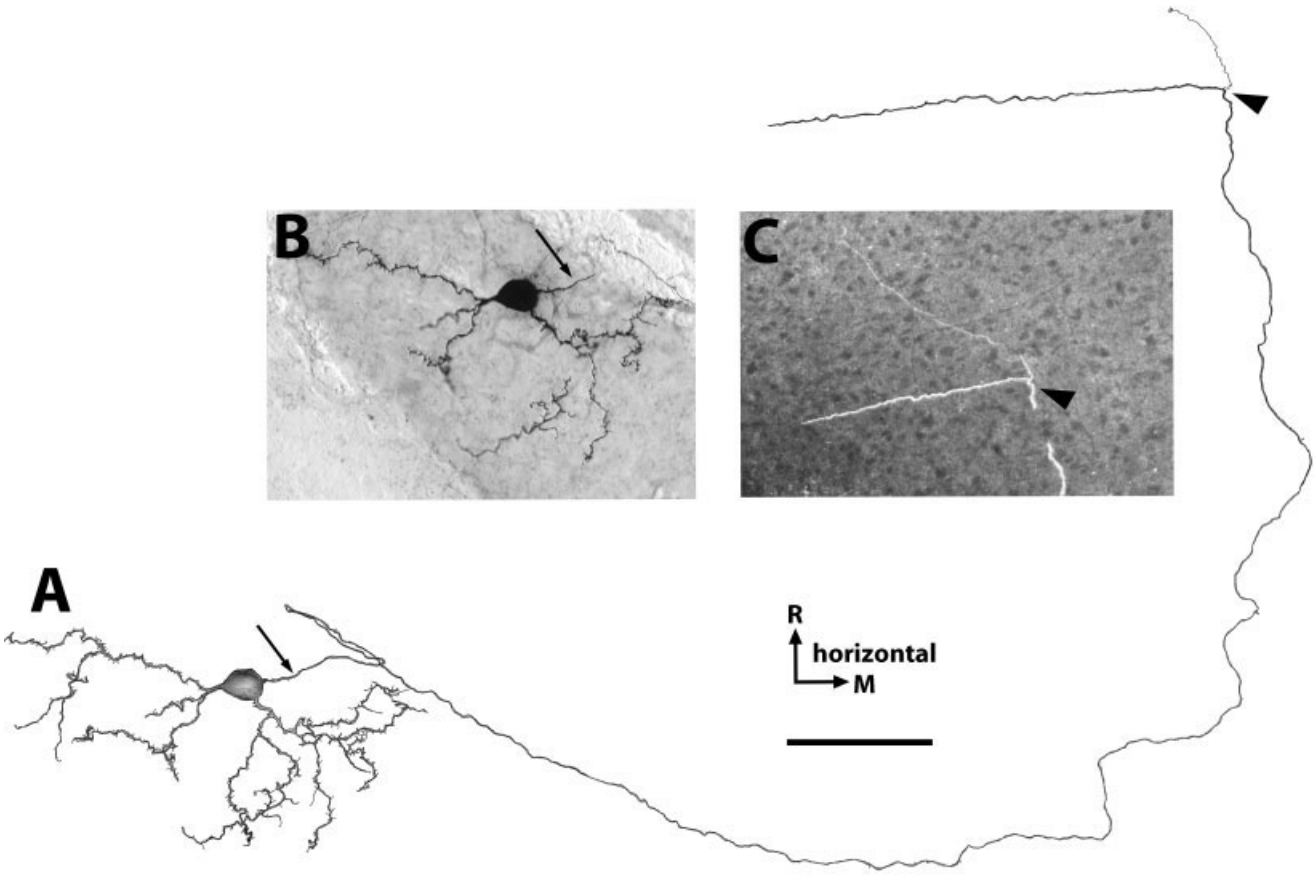

Fig. 13. Camera lucida reconstruction (**A**) and photomicrographs (**B,C**) of an intracellularly filled SLu neuron in the horizontal plane. Arrows indicate the primary axon and arrowheads indicate a fine collateral issuing from the primary axon. Scale bars = 100 μm in A (applies to A,B); 50 μm for C.

while some large-size boutons up to 2.2 μm in diameter were also found throughout layers. These large boutons were most frequently observed, although not consistently, in layer 3. Regardless of the variation of the bouton size, the highest density of boutons was always found in layer 5 and probably the adjacent layer 6.

The brush-like endings displayed some variations in their detailed morphology. Some endings demonstrated a distinctly laminated distribution of terminals and boutons with a predominately high density in layers 3–5 or 6 (for example, Fig. 5D). Others displayed a relatively uniform localization throughout layers 2–10, although layer 5 consistently contained the highest density of boutons (for example, Fig. 9). Figure 10 presents an example of two variations of Ipc endings overlapping in the same location but situated in different depths of the section. Two thick Ipc axons coursed adjacent to each other and issued many fine radial axonal collaterals in layers 7–10 before they arborized densely in more superficial layers 2–6 (Fig. 10B). In contrast, a third relatively thin axon was situated below the first two axons and remained smooth and unsplit in layers 7–10. The major arborization of the third axon started from layer 6 (Fig. 10C).

However, these variations do not simply imply distinct types of brush-like endings and may be either due to overlap of multiple endings or apical dendrites of labeled tectal neurons, can result from incomplete labeling of a structure, or may be caused by incomplete preservation of a structure in a section. Unfortunately, it could not be resolved whether these two variations in brush-like appearance shown in Figure 10 originated from one or two neurons, as the axons could not be traced back to the somata in Ipc. In order to unambiguously clarify the axonal terminal pattern of Ipc neurons within the TeO, individual neurons in Ipc with their distal axonal terminations were intracellularly filled in thick brain slices.

Complete axonal terminals of individual Ipc neurons were visualized in 1000-μm-thick slices in a tilted coronal plane, with the dorsal portion of the slice at a more rostral level than its ventral portion. These specially designed slices increase the opportunity of retaining caudally located somata and rostrally located axonal terminations of Ipc neurons in single slices. Three Ipc neurons with complete axonal terminations were successfully filled, with all three showing an identical morphology. Figure 11 illustrates one filled Ipc neuron which had a spiny columnar dendritic field (Fig. 11C) and a columnar brush-like ending in the TeO (Fig. 11A,B). The axon (2.7-μm-wide) emerged directly from the soma and its first segment was covered with short spines and processes and tapered with distance (Fig. 12I). The axon coursed laterally through Ipc and Imc and penetrated into the TeO at a 70° angle with

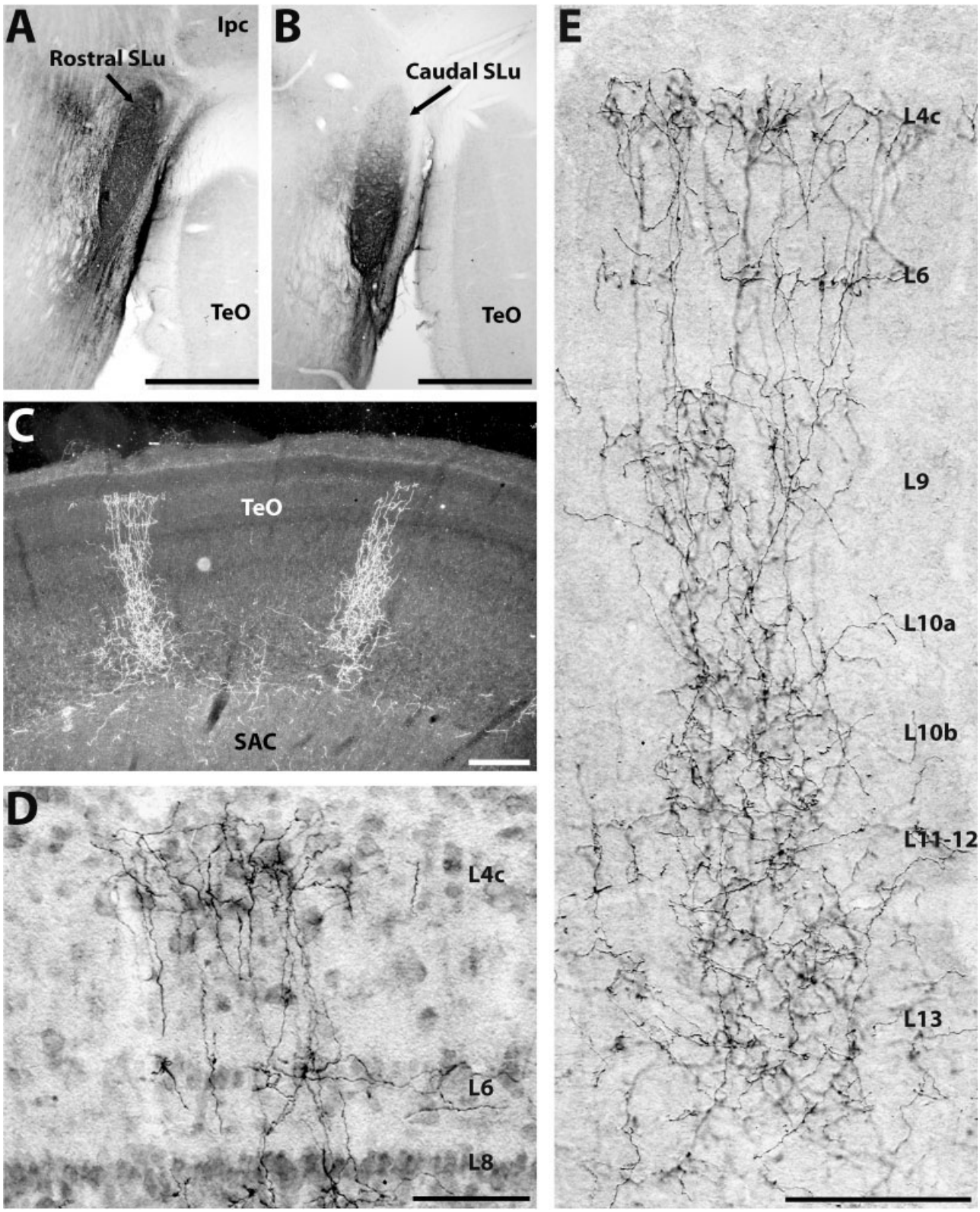

Fig. 14. Columnar axonal terminals within the TeO following an in vivo PHA-L injection into SLu. **A,B:** The injection involved the rostral (A) and caudoventral (B) portion of SLu. **C:** Darkfield image of the rostrolateral TeO with two labeled columnar structures extending from layer 13 to 4. **D:** Labeled neuropil in the superficial tectal layers 4–6 in a Giemsa-counterstained section. The most superficial layer appears to be layer 4c. **E:** Nomarski-DIC image of an individual SLu termination. Note distinct morphological segregation between superficial layers 4–8 and deeper layers 9–13. See Figure 1 for abbreviations. Scale bars = 500 μm in A,B; 200 μm in C; 50 μm in D; 100 μm in E.

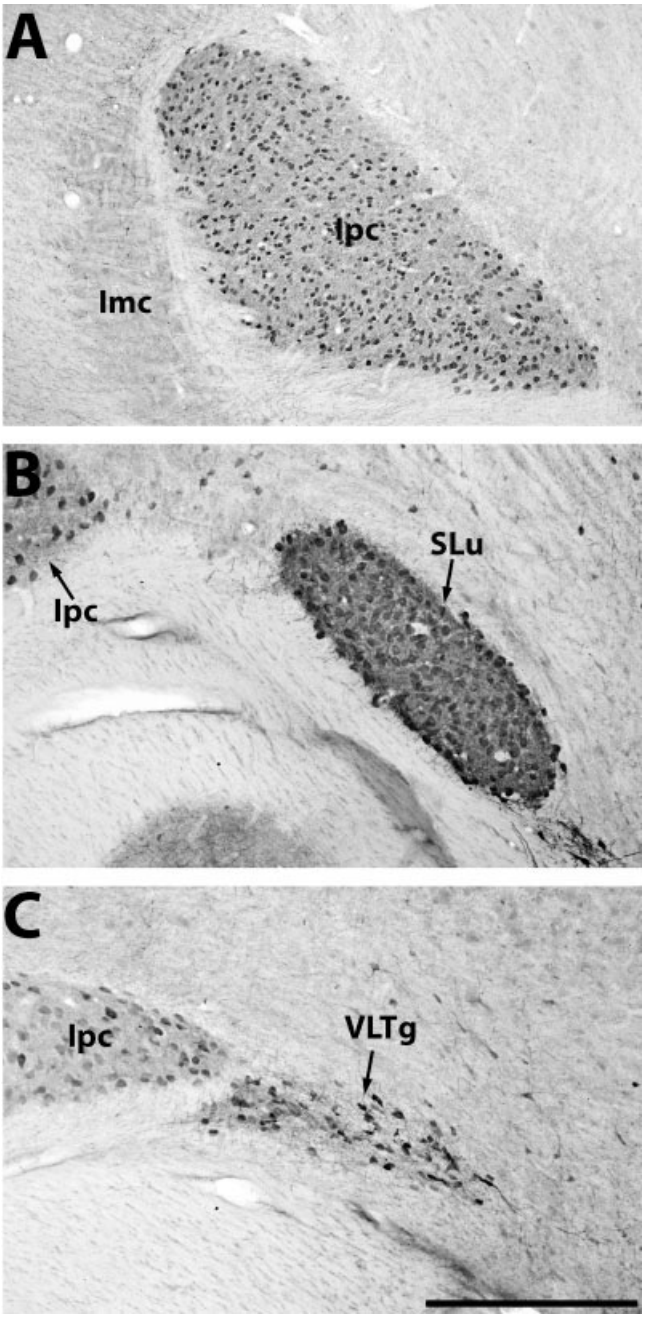

Fig. 15. ChAT immunoreactivity within Imc/Ipc (**A**), SLu (**B**), and VLTg (**C**). Ipc, SLu, and VLTg contained immunoreactive neurons, while none of Imc neurons were reliably labeled. Note a stronger intensity of the somatic and neuropil labeling in SLu compared to that in Ipc and VLTg. Scale bar = 500 μm in C (applies to A–C).

the tectal surface. The axon remained smooth and unsplit until it entered layer 13, where a fine collateral was issued and arborized diffusely in layers 11–13 and densely in layer 10 (Figs. 11A, 12H). Within layers 11–12, the main axon was divided into two parallel secondary branches which turned perpendicularly to the tectal surface in layer 10 (Fig. 11A). The secondary branches and their further ramifications formed a 50-μm-wide brush-like ending extending from layer 10 to 2 with differential morphologies among these layers (Fig. 11B). Layers 10–7 contained mainly radial thick axonal stems and a large number of fine branches that coursed parallel to each other (Figs. 11B, 12C). Layers 6–4 contained numerous laterally oriented fine arbors with several thick stems in the middle of the column (Fig. 12B), while layer 3 was filled almost exclusively with fine arbors (Fig. 12A). Only sparse arbors penetrated into layer 2.

A prominent feature common to both the diffuse arborization in the deeper layers (L11–13) and the columnar termination in the more superficial layers (L2–10) is very thick primary or low-order axonal stems (2–3 μm) giving off extremely fine branches less than half of a micrometer (for example, Fig. 12G,H). These fine branches and their distal arbors bore a high density of small boutons, 0.7–2.2 μm in diameter (Fig. 12D–F) in all tectal layers, with the highest density in layers 5 and 6. Two comparable dense bands were detected in the outer and inner portions of layer 5. Whether these two bands correspond to sublayers 5a and 5b requires further double staining for calbindin, the chemical marker that distinguishes these two sublayers from each other (Karten, unpubl. obs.). Layer 3 appeared to be the second-densest layer of axonal arbors and boutons. No obvious laminar distribution was detected based on the size of the axonal boutons.

Somatodendritic and local axonal morphology of SLu neurons. The morphology of SLu neurons was visualized by intracellular fillings of individual neurons in the coronal or horizontal planes (Fig. 13). All filled neurons in our preparations share similar somatodendritic and local axonal morphology. The soma was round or oval in shape with the long axis 18–30 μm and the short one 12–23 μm in length. Three to four primary dendrites ramified within a large field that tended to cover the whole mediolateral range of the nucleus (120–200 μm) and extended 200–300 μm in its dorsoventral dimension. Both primary and distal dendrites were covered with a high density of filiform spines. Although the primary axon could not be reliably detected in some neurons, other neurons issued a smooth axon directly from the soma and usually coursing medially or ventrally. Figure 13 illustrates a typical SLu neuron in the horizontal plane whose axon could be traced dorsally to the level of the nucleus tegmenti pedunculo-pontinus, pars compacta (TPc; Kuenzel and Masson, 1988) where the primary axon turned laterally toward the optic lobe after giving off a fine collateral extending dorsally. Terminal distribution and morphology of the individual SLu axons could not be visualized in any of the intracellularly filled neurons due to the lengthy and changing course of their axons from their origins in SLu to their terminations within the TeO.

Distal axonal morphology of SLu neurons within the TeO. The morphology of the distal axonal terminations of SLu neurons within the TeO was examined with in vivo tracing studies. Following in vivo CTB injections into SLu, densely labeled neuropil in the TeO was found in layers 11–13, 9, 6, and a sublayer along the border between layers 4 and 5 (Fig. 6B). This most superficial sublayer appeared to be layer 4c in most cases. However, in some portions of the TeO, especially the dorsal portion, the boundary between layers 4c and 5a was hard to establish without additional chemical markers. Within the contralateral TeO, sparse terminals were found in the deep layers, which were not detected following a more precise

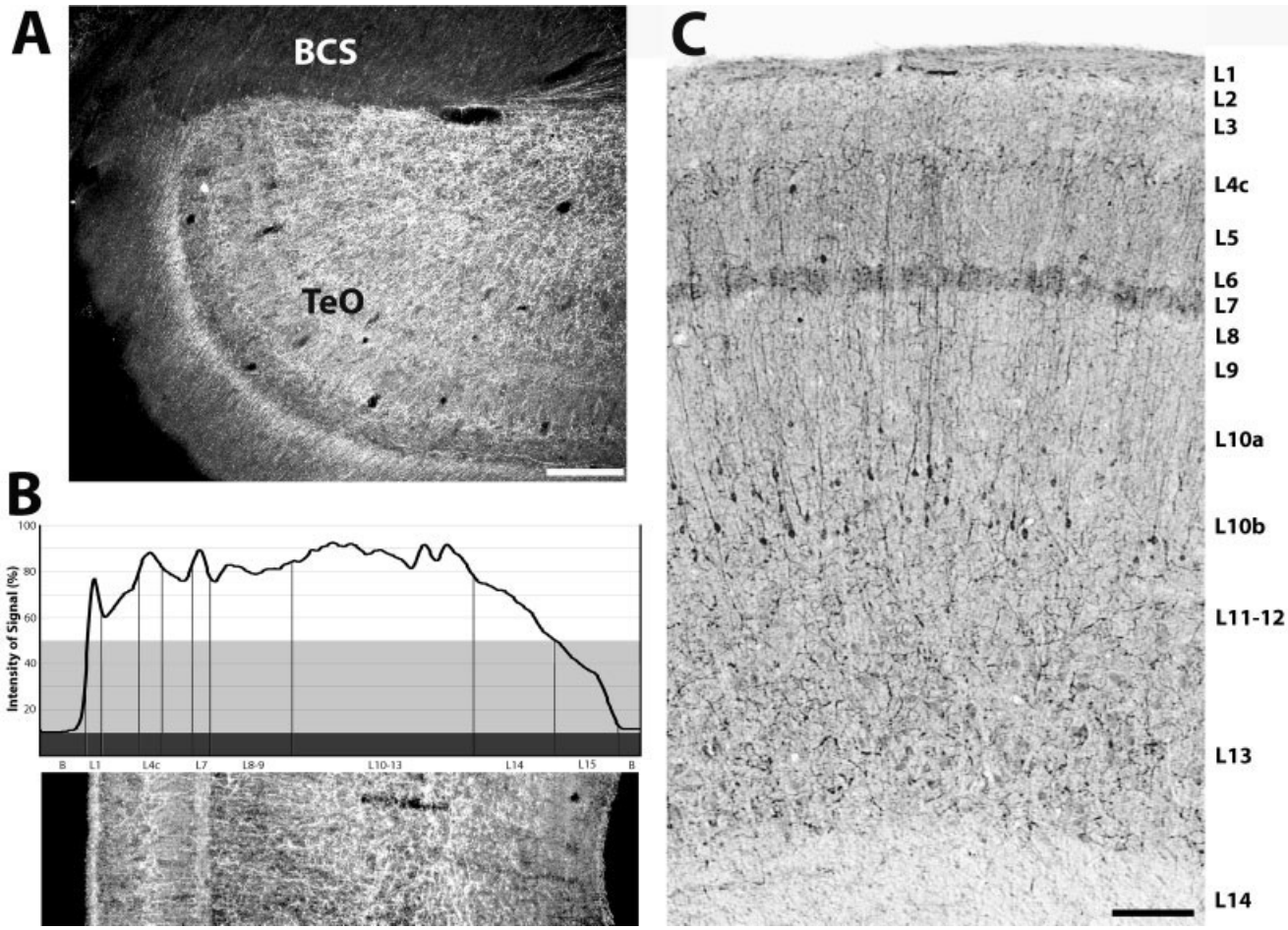

Fig. 16. ChAT immunoreactivity within the TeO. **A:** Darkfield image through the most ventromedial portion of the TeO. The whole range of the TeO contains dense immunoreactive neuropil, in contrast to the sparse staining in BCS. **B:** Histogram of the signal intensity (up) among layers in the lateral portion of the TeO (bottom). Dark gray zone in the histogram corresponds to the background outside the TeO and the VT. Light gray zone corresponds to the tectal layer 15 which does not contain substantial staining. All other tectal layers contain dense immunoreactivities, indicated by the white zone above the light gray level. Note several signal peaks in layers 1, 4c, 7, 10, and 13. **C:** Brightfield view of the lateral TeO illustrating immunoreactive neurons mainly located in layer 10. Scale bars = 200 μm in A,C.

injection into SLu with PHA-L. In vivo PHA-L injections into SLu revealed the columnar organization of axonal terminations of SLu neurons within the TeO, consistent with a previous report in pigeons (Brecha, 1978). Figure 14 illustrates the anterograde label within the TeO following an injection into the rostral (Fig. 14A) and caudoventral (Fig. 14B) portions of SLu. Leakage of tracer was found in a small area dorsomedial to SLu. Although PHA-L was mainly transported in an anterograde direction, weakly labeled retrograde neurons were detected in Imc but not in TeO (not shown). Anterogradely labeled fibers and terminals were found mostly in the rostral portion of the ipsilateral TeO and organized in columns (Fig. 14C). The columns were about 120–180 μm wide and extended from layer 4c to 13 with dense arborizations in layers 4c, 6, and 9–13. In contrast to the combination of very thick axonal stems and extremely fine spiny arbors of Ipc brush-like endings, the labeled columnar structures followed PHA-L injections into SLu consisted of smooth axonal arbors of the same caliber (0.5–0.8 μm). No obvious boutons were detected on these axonal arbors. The terminal pattern of individual columns differed in deep tectal layers 9–13 and more superficial layers 4c–8 (Fig. 14D,E). Arbors in layers 9–13 coursed in a curving and seemingly random fashion, without preferred orientation. Layers 4c–8 contained mostly parallel radial arbors passing through the major portion of layer 5, 7, and 8, and arborizing in layers 4c and 6. In some cases the superficial portion of the column seemed to extend slightly wider than the deep portion. The densest arborization of the whole column occurred in layers 10b–13.

Biochemical features of isthmic neurons

Distribution of various histochemical and immunocytochemical staining within the nucleus isthmi and the TeO was examined to explore the possible biochemical substrate of the tecto-isthmic circuitry, as well as to reveal the different nature of neurons in Imc, Ipc, SLu, and VLTg. In contrast to the negative somatic staining in Imc, neurons in Ipc, SLu, and VLTg were darkly labeled for ChAT (Fig. 15). Within the TeO, ChAT-immunoreactive neuropil displayed a wide distribution and occupied all tectal layers with the

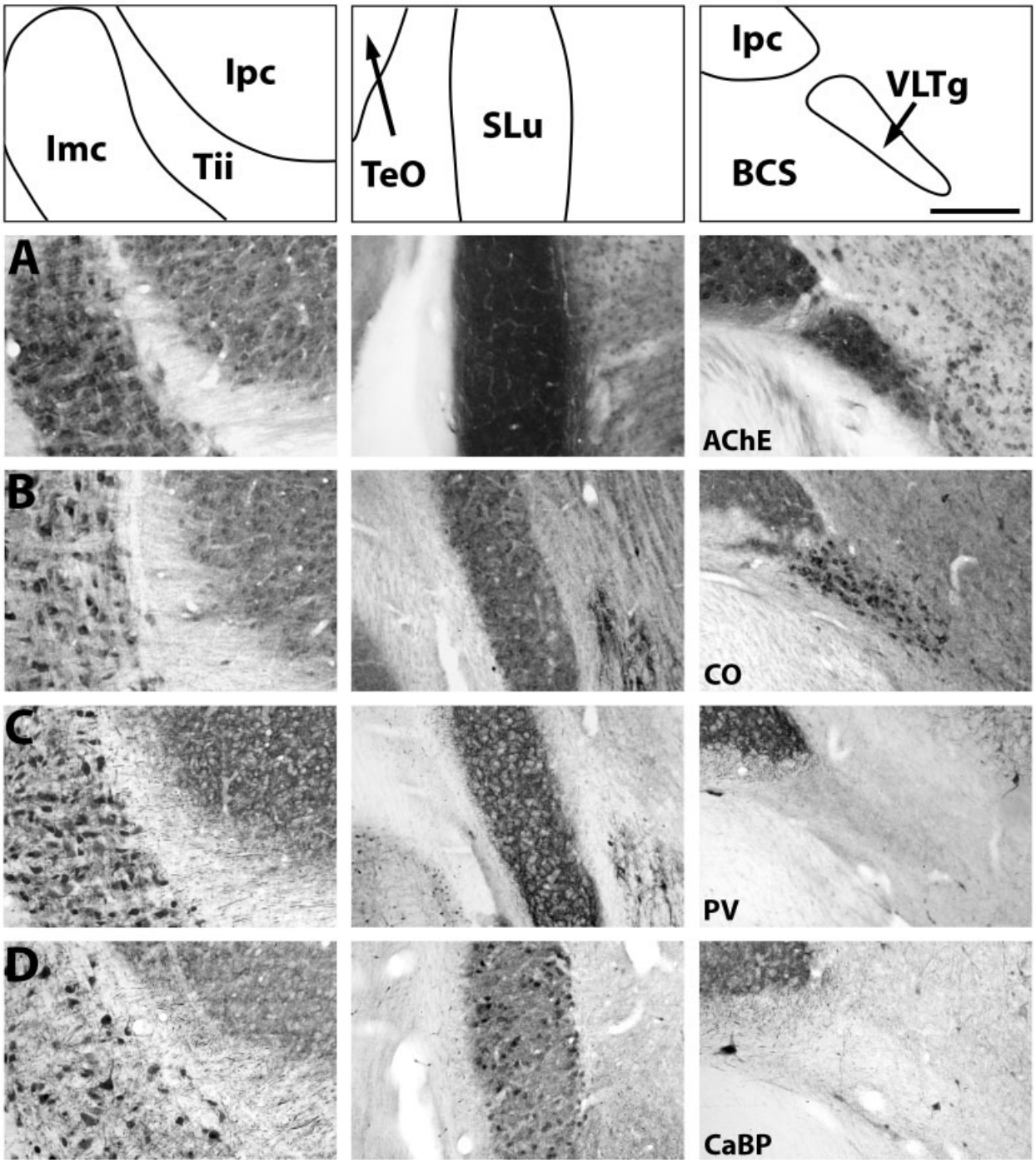

Fig. 17. Distribution of AChE (**A**), CO (**B**), PV (**C**), CaBP (**D**), and nAChRs (**E–G**) in Imc/Ipc (left column), SLu (intermediate column), and VLTg (right column). Boundaries and relative location of the isthmic nuclei are illustrated in the line drawings at the top. Imc, Ipc, SLu, and VLTg exhibited differential neuropil and somatic staining. See details in the text. Scale bar = 200 μm (applies to all panels).

exception of the stratum griseum periventriculare (layer 15; Fig. 16). Sublayer 4c, corresponding to the most superficial layer of the SLu axonal terminations, contained conspicuous ChAT-immunoreactive coarse arbors. Layers 6–2 were composed of numerous extremely fine granular particles and relatively thick radial processes. ChAT-immunoreactive neurons were located mainly in layer 10 and scattered in layers 3, 4, 5, 9, and 13 (Fig. 16C). These neurons were morphologically different from the tecto-isthmic neurons and did not show shepherd's crook axons. However, considering the incomplete staining of the cellular morphology in ChAT immunocytochemistry, clarification of the proposed

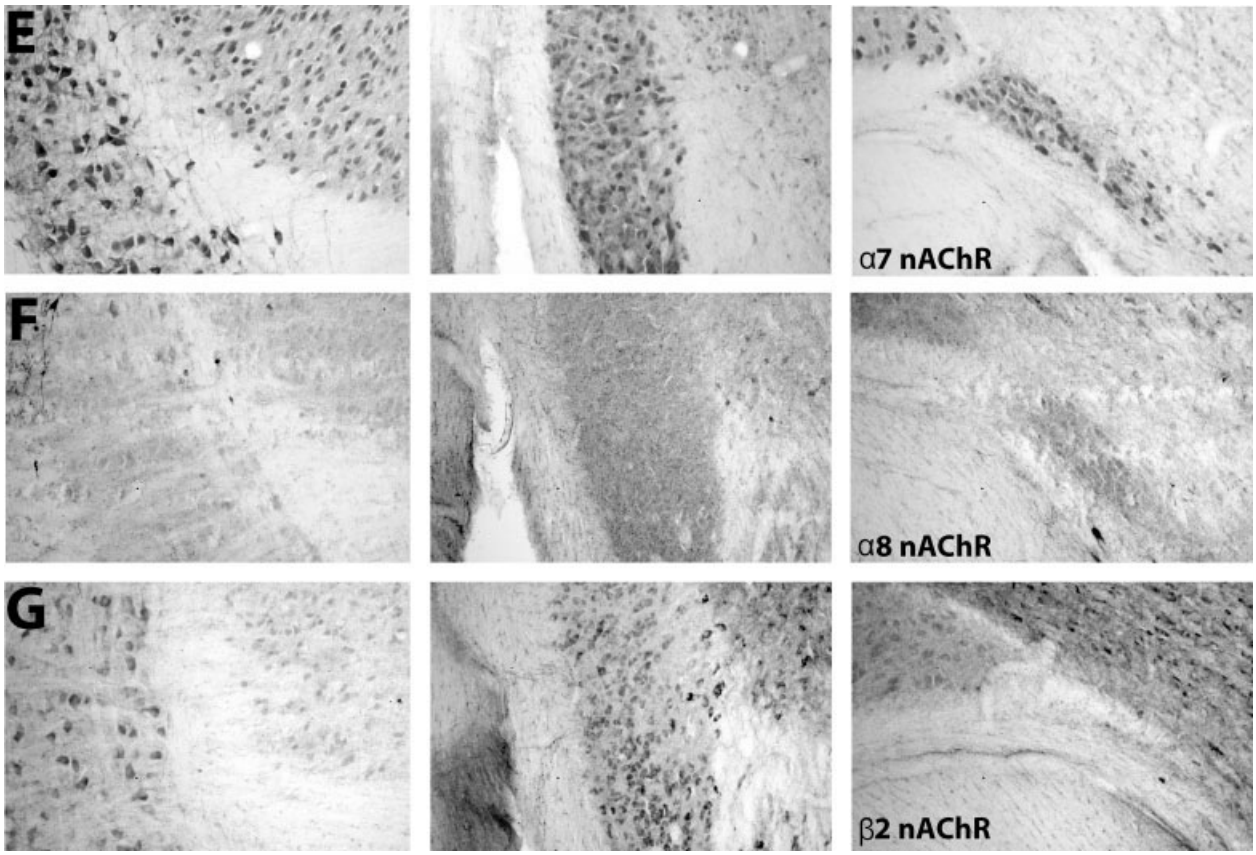

Figure 17 (Continued)

cholinergic inputs to the nucleus isthmi in birds requires further double label for ChAT immunocytochemistry and retrograde tracing studies.

In AChE histochemical staining (Fig. 17A), both neuropil and cells within Imc, Ipc, SLu, and VLTg were darkly stained. A more intense staining was found in SLu than in Imc, Ipc, and VLTg. In cytochrome oxidase histochemical staining (Fig. 17B), cells in Imc and VLTg were conspicuously labeled against relatively light staining in the surrounding neuropil. In contrast, Ipc and SLu exhibited a strong neuropil staining with lightly labeled cells.

Various isthmic nuclei displayed a distinct pattern of immunoreactivity for parvalbumin and calbindin (Fig. 17C,D). Imc contained both parvalbumin-immunoreactive and calbindin-immunoreactive neurons against a lightly labeled background. In contrast, darkly labeled neuropil for parvalbumin and calbindin surrounded unlabeled cell bodies in Ipc. Within SLu, neuropil was immunoreactive for both parvalbumin and calbindin while cell bodies were only labeled for calbindin. Neither cells nor neuropil in VLTg contained immunoreactivity for parvalbumin or calbindin, providing unambiguous evidence of a unique difference between VLTg and the isthmic nuclei.

Imc, Ipc, SLu, and VLTg were equally notable in their intense immunoreactivity for α7 nAChR (Fig. 17E) and their lack of immunoreactivity for α8 nAChR (Fig. 17G). They differed from each other in the pattern of β2 nAChR immunocytochemical staining (Fig. 17F). Neurons were moderately labeled in Imc and SLu and lightly labeled in Ipc. No staining for β2 nAChR was detected in VLTg.

Immuncytochemical staining for the fast voltage-gated potassium channel Kv3.1 revealed intense neuropil staining surrounding the unlabeled cell bodies in Imc, Ipc, and SLu (Fig. 18A,C–E). While in SLu and Ipc the neuropil staining was rather diffuse (Fig. 18D,E), the outline of the large Imc neurons could clearly be differentiated due to the dense studding with immunoreactive profiles (Fig. 18C). Within the TeO, labeling was found in a population of radial neurons in layer 10b (Fig. 18B). The somata and the apical primary dendrites were well outlined; however, labeling decreased in the more distal aspects of the dendritic field, and thus did not allow identification of a shepherd's crook morphology. We could not precisely determine whether labeled structures were located on afferent axons (i.e., presynaptically) or within the tectal neurons (i.e., postsynaptically).

DISCUSSION

Columnar axonal terminations of Ipc and SLu neurons

The major contribution of the current study is the confirmation of the columnar organization of the axonal termination of Ipc and SLu neurons within the TeO at the individual cell level and a detailed description of their

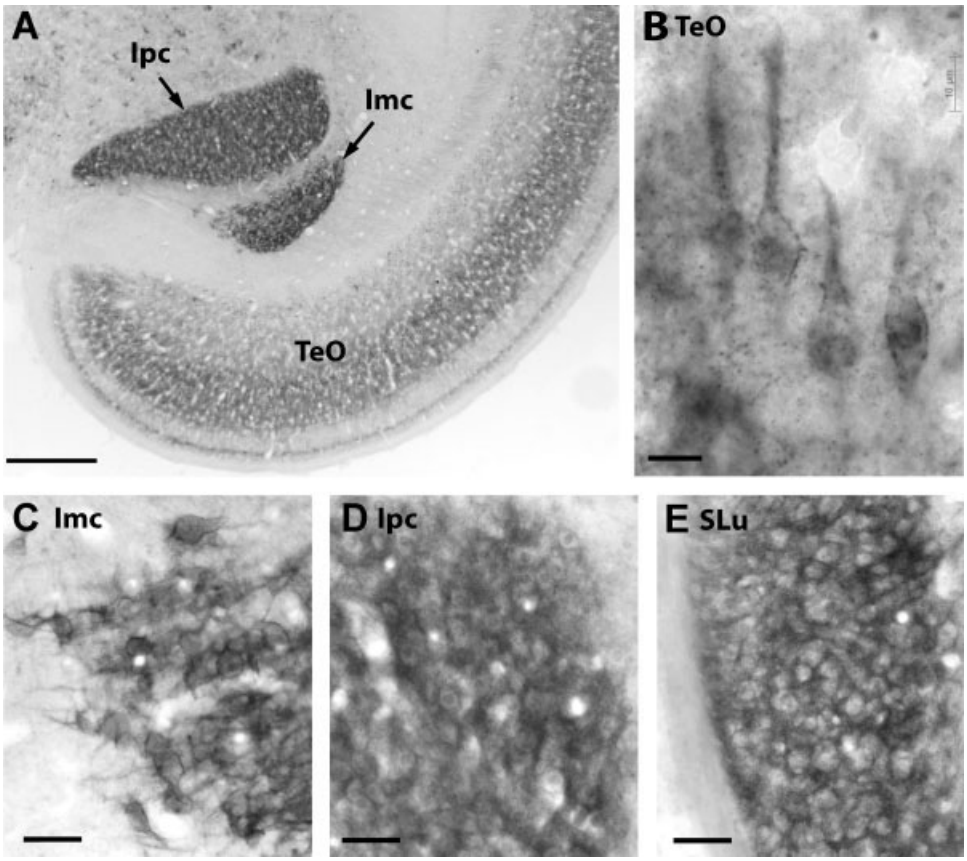

Fig. 18. Immunoreactivity of Kv 3.1 in the TeO, Imc, Ipc, and SLu. **A:** An overview of the TeO, Imc, and Ipc. **B–E:** Higher-power view of neurons in tectal layer 10 (B), Imc (C), Ipc (D), and SLu (E). Imc, Ipc, and SLu all contained intense neuropil staining while their neurons were unlabeled. Scale bars = 500 μm in A; 10 μm in B; 50 μm in C–E.

morphology. Individual Ipc neurons terminate densely in the superficial layers 3–6, moderately in the intermediate layers 7–10, and lightly in the deep layers 11–13. Their termination in the superficial and intermediate layers is organized in a narrow brush-like column, consistent with previous reports (Ramón y Cajal, 1899, 1911; Brecha, 1978; Tömböl et al., 1995; Tömböl and Németh, 1998). A terminal varicosity in layer 10 described by Ramón y Cajal (1911) in sparrows was not seen in the current study. Two major variations of Ipc brush-like endings were observed in the current tracing studies and may correspond to the long and short axonal arborizations identified by Tömböl et al. (1995, 2005; 1998), although our observation does not support their previous suggestion that short and long endings, respectively, arise from Ipc and Imc. The light, diffuse projection from Ipc on the deep tectal layers 11–13 was first identified in our PHA-L tracing studies and further confirmed with intracellular filling of individual Ipc neurons.

The current study visualized individual columnar axonal terminations of SLu neurons and clarified the previously controversial reports in their laminar distribution (Brecha, 1978; Hellmann et al., 2001). These terminations extend from layer 13 superficially to layer 4c. Arborization occurs in layers 4c, 6, and 9–13, with a higher density in layers 10b–13 than in the more superficial layers. Autoradiography experiments in pigeons identified a comparable dense innervation of SLu axons to tectal layers 6–13 in a radial fashion but not as superficial as to layer 4c (fig. 29 in Brecha, 1978). This discrepancy may be due to technical limitations (see Cowan and Cuénod, 1975) or interspecies variation. The latter possibility is supported by the different pattern of cholinergic fibers in the layer 4c between these two avian species. In chicks, layer 4c contains coarse cholinergic arbors, while these cholinergic arbors are lacking in the corresponding layer in pigeons (fig. 18 in Medina and Reiner, 1994; Wang and Karten, unpubl. obs.). However, unambiguous confirmation of the laminar distribution of SLu neurons still requires intracellular filling experiments.

In addition to the coarsely separate laminar domains, columnar axonal terminations of Ipc and SLu axons differ in several important morphological features, including the width of the column, the thickness of axonal arbors, and the density of axonal boutons. Individual columnar terminations of SLu neurons (120–180 μm) are two to three times wider than Ipc brush-like endings (35–50 μm). Ipc brush-like endings possess very thick axonal stems (2–3 μm) surrounded by extremely fine arbors (less than 0.5 μm), while SLu terminations are composed of coarse axonal arbors of the same caliber (0.5–0.8 μm). Furthermore, Ipc axons carry a high density of small boutons on their distal fine arbors, while SLu axons and their distal arborizations are almost free of obvious boutons.

Ipc and SLu provide a major contribution to the tectal ChAT and AChE

Both the somata of Ipc and SLu neurons and their distal axonal terminations within the TeO display a strong immunoreactivity for choline acetyltransferase (ChAT), a re-

liable marker for the presence of cholinergic systems. Considering the dense termination and extensive laminar distribution of the Ipc and SLu efferents in the TeO, as well as the glutamatergic nature of the retinal inputs (Wang et al., 1978; Dye and Karten, 1996), Ipc and SLu may provide a substantial contribution to the tectal cholinergic system. In addition, Ipc and SLu may also contribute to the tectal cholinesterase (AChE). The presence of high concentrations of AChE in the TeO of all vertebrates has long been recognized (for example, birds: Scharrer and Sinden, 1949; mammals: Ross and Godfrey, 1985; reptiles: Schmidt et al., 1989; amphibians: Wallace et al., 1990). Retinal inputs provide a contribution to the presence of AChE in the superficial TeO. Unilateral ocular ablation results in a detectable reduction, but not a complete loss, of the tectal AChE staining in birds, reptiles, and amphibians (Ciani et al., 1978; Ciani and Franceschini, 1982; Wallace et al., 1990; Villani and Contestabile, 1982; Karten, unpubl. obs.). The residual AChE staining may be due to AChE content within axons of Ipc and SLu that terminate in these layers of the TeO. In frogs, retinal and bilateral nucleus isthmi deafferentiation leaves virtually no AChE activity in the outer tectal layers (Wallace et al., 1990).

What are the postsynaptic targets of Ipc and SLu?

Although physiological studies reported a dramatic influence of the nucleus isthmi on visual responses and the receptive field organization of tectal neurons (Wang SR et al., 1995; Wang Y et al., 2000), the target neurons of the isthmotectal terminals have not been identified so far. As any suggestion on the role of the isthmi nuclei in tectal function requires identification of the specific targets, more detailed analysis with electron microscopy, immunocytochemistry, and cell filling, as well as single-cell electrophysiology, is required. Specifically, the synaptic relationship between isthmotectal terminals and retinotectal terminals remains obscure (see discussion in Gruberg et al., 1994). Within the TeO there is a lack of presynaptic profiles on retinal axonal endings (for example, Hayes and Webster, 1975; Hughes, 1990; Udin et al., 1990; Gruberg et al., 1994). However, there are two reasons to entertain the possibility of a direct action of the isthmotectal terminals on the retinotectal terminals. 1) Several studies have reported significant effects of cholinergic isthmic inputs on the retinotectal neurotransmission. Activity of the nucleus isthmi enhances calcium influx into optic nerve fiber terminals (Dudkin and Gruberg, 2003), enhances the long latency component of retinotectal transmission (King and Schmidt, 1991), and sharpens the tectal retinotopy (Schmidt, 1995). Unilateral lesions of the frog nucleus isthmi result in a scotoma in the contralateral monocular field (Gruberg et al., 1991). 2) Titmus et al. (1999) reported that nicotinic receptors are present on retinotectal axons and activation of those receptors increases spontaneous release of glutamate, a major neurotransmitter used in the retinotectal projection. The rich presence of nicotinic receptors in retinal ganglion cells does not correlate with the intraretinal arborization of their dendrites in relationship to the laminar distribution of cholinergic amacrine cell processes. Thus, the retinal ganglion cells expressing these receptors may indicate that their axons utilize these receptors, and are influenced by cholinergic inputs at their central terminations. An interesting hypothesis that might resolve this issue was put forward by Sargent et al. (1989), who suggested a nonclassical, paracrine action of cholinergic input to the TeO. This interpretation is corroborated by the columnar morphology of isthmic terminals that do not show a concentration on a target structure, but are rather homogeneously distributed.

Tectal inputs to Ipc and SLu

Another major finding of the current study is that tectal input to Ipc and SLu arises from a particular cell population located in the same sublayer of the TeO. Double-labeling studies have revealed that these neurons are immunoreactive for antibodies against the transcription factor Brn3a in layer 10b. Although the functional significance of this factor in the tectum remains unknown, our observation suggests that layer 10 is a heterogeneous layer and only a particular cell population in layer 10 is responsible for the tectal inputs on the nucleus isthmi. These neurons do not correspond to three types of radial neurons in layer 10 with side dendritic branches in layer 7 identified by Sebestény et al. (2002, see discussion in Wang et al., 2004). The radial tectal neurons with side-branches in layer 7 were not encountered in our experiments following both in vivo and in vitro tracing studies in Ipc and SLu. Rather, neurons with such a morphology were labeled after CTB injections into the nucleus geniculatus lateralis pars ventralis (Mpodozis and Karten, unpubl. obs.). However, it remains unknown whether it is the same population of tectal neurons that innervates both Ipc and SLu. Tectal axons terminate in a restricted columnar fashion in both Ipc and SLu (Hunt and Künzle, 1976; Streit et al., 1980; Güntürkün, 1987). The widespread tectal terminals within Ipc reported by Ramón y Cajal (1911, fig. 139) rather resemble the pattern of Imc arborizations (see Wang et al., 2004).

There is physiological evidence that acetylcholine and/or glutamate play important roles in the tecto-isthmic transmission (Felix et al., 1985; Wu et al., 1994; Wang, 2003). The avian Imc, Ipc, and SLu show a strong somatic staining for α7 subunit of nicotinic acetylcholine receptors (Britto et al., 1992) and glutamate receptor subtypes GluR1 or GluR2/3 (Hellmann et al., 2001). However, ChAT-immunoreactive neurons appear morphologically different from the TeO-Ipc neurons. Clarification of the neurotransmitter used in this pathway requires further investigation with a combination of physiological, tract-tracing, and immunocytochemistry studies.

Ipc and SLu are two closely related but independent nuclei

On the basis of the data presented here, the organization, connection, and biochemical features of Ipc and SLu can be compared (Table 1). Our study confirmed the obvious similarities of Ipc and SLu in the general pattern of their cytoarchitecture, cell morphology, connection, and some biochemical features, and further revealed their distinct features. The most important feature that distinguishes Ipc and SLu from each other is the distinct morphology and laminar distribution of their columnar axonal terminations in the TeO. In addition, Ipc and SLu differ in the precision of their topographical relationship to the TeO, dendritic shape and orientation, and calbindin-immunoreactive cells in SLu, which is lacking in Ipc. These distinct features have resolved the seeming paradox of the identical pattern of the Ipc and SLu, indicating their

TABLE 1. Comparison of the Cell Morphology, Connections, and Biochemical Features of Ipc and SLu[1]

	Similarities	Differences	
		Ipc	SLu
Cell morphology	Small round or oval cells Spiny dendrites	Uniform distribution Narrow radial dendritic pattern	Cell clusters Large dendritic field without preferred orientation
Imc input	GABAergic input from single Imc axon upon both Ipc and SLu		
Relationship to the TeO	Homotopic reciprocal connected with the ipsilateral TeO Same topography	Precise	Relatively diffuse
Tectal input	Radial neurons in layer 10b Brn3a immunoreactive neurons	Shepherd's crook axons	Unknown
Axonal terminations within the TeO	Columnar organization	Brush-like endings rich in boutons 35–50 μm wide Extending in layers 2–10 An additional diffuse arborization in layers 10–13	Arbors of same caliber lack in boutons 120–180 μm wide Extending in layers 4c–13 —
Other efferent targets		None	Pretectum and thalamus (Hellmann et al., 2001)
Biochemical features	AChE:cell bodies (++); neuropil (+++) CO: cell bodies (+); neuropil (++) GABA: cell bodies (–); neuropil (+++) PV: cell bodies (–); neuropil (+++) α7 nAChR: cell bodies (+++); neuropil (?) α8 nAChR: cell bodies (–); neuropil (–) KV 3.1: cell bodies (–); neuropil (+++)	ChAT: cell bodies (++); neuropil (?) CaBP: cell bodies (−); neuropil (++) GluR1: cell bodies (−) GluR2/3: cell bodies (++) β2 nAChR: cell bodies (+); neuropil (−)	ChAT: cell bodies (+++); neuropil (?) CaBP: cell bodies (+, scattered); neuropil (++) GluR1: cell bodies (+++) GluR2/3: cell bodies (−) β2 nAChR: cell bodies (++); neuropil (−)

[1]The similarities and differences between Ipc and Slu indicate that they are two closely related but independent cell groups; +++, heavy staining; ++, moderate staining; +, light staining; –, none; ?, uncertain.

parallel and independent roles in the isthmotectal interactions.

Is VLTg another isthmic nucleus?

In addition to Ipc and SLu, the current study has confirmed another cholinergic cell group ventromedial to Ipc and rostral to SLu that was first identified by Sorenson et al. (1989). The current study termed this cell group the nucleus ventrolateralis tegmenti (VLTg). VLTg shares many features with Ipc and SLu, but differs in its conspicuously labeled cells for cytochrome oxidase and the total lack of immunoreactivity for parvalbumin, calbindin, and β2 nAChR. While Sorenson et al. (1989) reported a cholinergic connection between SLu and VLTg, we did not find such a projection or a connection with the TeO, indicating that VLTg is not a simple extension of Ipc and SLu. In addition, VLTg is not consistent with the description of other small cell groups which have been suggested to be related to the isthmic system, including the *disseminated isthmic nucleus,* which is located dorsally to Ipc and projects on the ipsilateral TeO (see fig. 19 in Medina and Reiner, 1994; previously called the *nucleus lemnisci lateralis, pars dorsalis* in Karten and Hodos, 1967), and the *nucleus isthmi ventralis,* which projects on the contralateral TeO (Vaage, 1973; Martinez and Puelles, 1989; also see discussion in Wang et al., 2004). Whether the VLTg is an independent isthmic nucleus, or completely unrelated to the isthmic system requires further studies.

Identical nuclei and pathways in the mammalian brain

The Ipc and SLu, collectively, appear to be homologous to the nucleus parabigeminalis of the mammalian brain (Le Gros Clark, 1933; Diamond et al., 1992). Neurons in the nucleus parabigeminalis are reciprocally connected with the superficial layers of the superior colliculus, the homologous structure of the nonmammalian TeO (Harting et al., 1973; Graybiel, 1978; Sherk, 1979a; Méndez-Otero et al., 1980; Major et al., 2003). As in birds, reptiles, amphibian, and teleosts, most neurons in the nucleus parabigeminalis are cholinergic (Mufson et al., 1986; Hall et al., 1989; Jeon et al., 1993). Although the nucleus parabigeminalis appears to be a uniform structure in cats and ferrets (Graybiel, 1978; Baleydier and Magnin, 1979; Edwards et al., 1979; Sherk, 1978, 1979a,b; Roldán et al., 1983; Jiang et al., 1996), it is divided into two or three cytoarchitectonically distinct subdivisions in the squirrel and rat (Tokunaga and Otani, 1978; Watanabe and Kawana, 1979; Linden and Perry, 1983; Wang and Karten, unpubl. obs.). In squirrels, two subdivisions of the nucleus parabigeminalis maintain independent sets of reciprocal connections with the ipsilateral superior colliculus and terminate in a columnar fashion (Wang and Karten, unpubl. obs.), resembling the relationship of Ipc and SLu to the avian TeO.

Functional implications of the isthmotectal interaction

Reciprocal connections between the TeO and the nucleus isthmi consist of one heterotopic GABAergic and two homotopic cholinergic feedback components (Fig. 19). The most remarkable feature of the homotopic components is the columnar organization of the efferents from Ipc and SLu that extend over many tectal layers. These columns constitute juxtaposed cartridges throughout the TeO that contain a single termination of Ipc or SLu axons, their postsynaptic target structures, and other extrinsic inputs to these targets. Since every element contained within such a cartridge samples the same small region of the visual field, the function of the cholinergic Ipc and SLu axons might be the synchronization of excitation across one cartridge. In contrast, the heterotopic GABAergic component of the isthmotectal interaction consists of widely spreading terminals of Imc neurons that might inhibit the Ipc/SLu neurons that project on the TeO. Taken together, both systems constitute a complex mech-

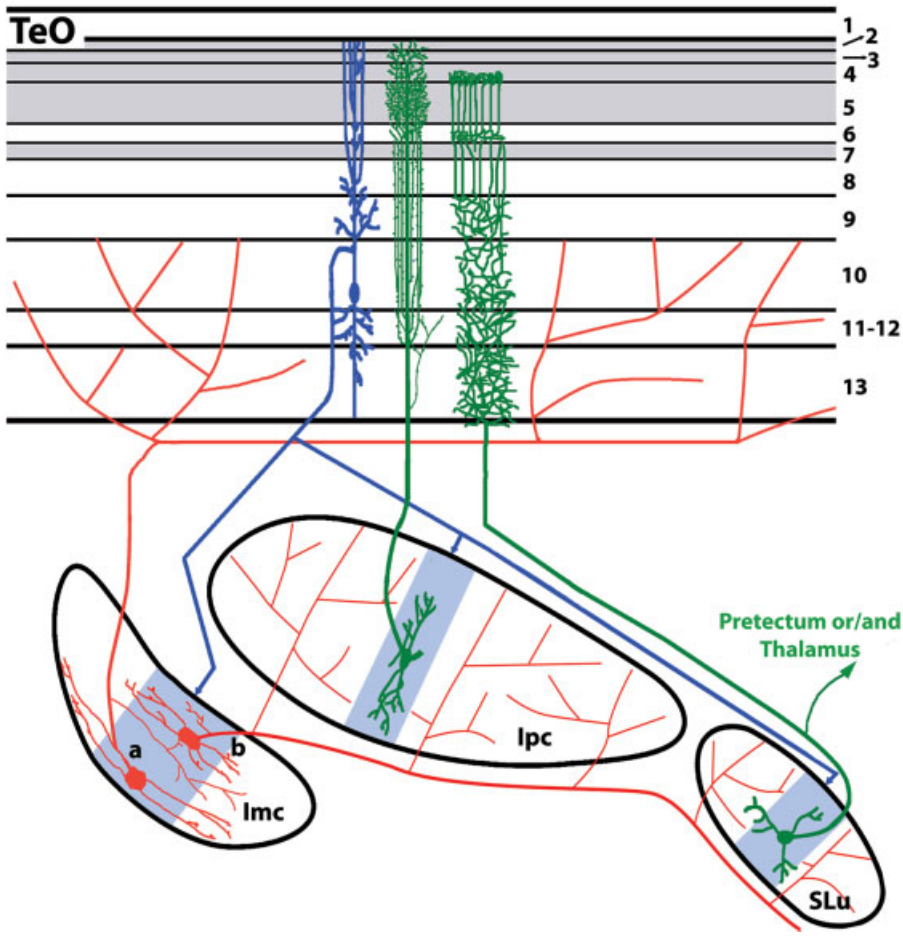

Fig. 19. Schematic drawing of the neuronal circuitry of the TeO, Imc, Ipc, and SLu. Radial tectal neurons (blue) in layer 10b project topographically on Imc, Ipc, and SLu. Imc-Is neurons (a, red) and Imc-Te neurons (b, red) project widely on Ipc/SLu and the TeO, respectively. Ipc and SLu axons (green) terminate within different tectal layers in a columnar fashion. The gray shadings of the TeO indicate retinorecipient tectal layers. The blue shadings within Imc, Ipc, and SLu indicate the tectal terminal projection.

anism to enhance excitation and inhibition in specific tectal domains. Whether this network is fundamental for the implementation of a "winner-take-all" network or for the production of center-surround receptive field organization in tectal neurons is still unclear.

The finding that a high-threshold (Kv3.1) voltage-activated potassium channel is expressed by all isthmic nuclei is consistent with a function in the time domain. In avian brains, this ion channel has been reported predominantly in structures of the auditory system dedicated to time-coding (Parameshwaran et al., 2001; Lu et al., 2004). The members of the Kv3 subfamily of voltage-activated potassium channels activate rapidly at potentials positive to –10 mV and allow for the rapid repolarization after an action potential, a feature that enables high-frequency firing and improves postsynaptic temporal coding precision (Wang et al., 1998). This function is essential for the time-coding circuits in the auditory brainstem, and could also relate to the high-frequency oscillations in the tectum that were reported to be mediated by the isthmic system (Marín et al., 2005).

Although the exact targets of Ipc and SLu axons remain unknown, the high concentration of Ipc synaptic boutons in layers 3–6 imply that structures contained in these layers could be its primary targets. Distal dendritic arbors of tectal ganglion cells (TGCs) of layer 13 might be such a target. TGCs are the main ascending output of the TeO on the thalamus, and since the nucleus isthmi is involved in modulation of tectal activities, an interesting possibility is a direct action from the nucleus isthmi on the tectal ascending system.

TGCs have large dendritic fields and generate large arrays of small columnar dendritic endings (bottlebrush endings) positioned in specific tectal layers, (Luksch et al., 1998, 2001; Major et al., 2000). Based on the laminar position of the bottlebrushes, several subtypes of type I TGCs have been identified in chicks (Luksch et al., 1998) and in pigeons (Hellmann and Güntürkün, 2001; Marín et al., 2003). As subtle interspecies variations in the laminar distribution of both isthmic terminations and TGCs bottlebrushes may exist, we will discuss the functional implications only for the chick where most of the relevant structures have been analyzed at the single-cell level. In chicks, bottlebrushes of type I TGCs are monostratified in retinorecipient tectal layers 5a, 5b (Luksch et al., 1998) and probably layer 3 (Brzozowska-Prechtl and Karten, unpubl. obs.), where Ipc brush-like endings densely terminate. Type II TGCs have endings stratified in deeper nonretinorecipient layer 9 that are also significantly innervated by Ipc endings, although to a greatly reduced degree.

Some possible insight into the operational domains of the Ipc terminals is suggested by the dimensions of their arbors (Fig. 20A,C). Individual brush-like endings of Ipc neurons are 35–50 μm wide. Each bottlebrush ending in layer 5a and

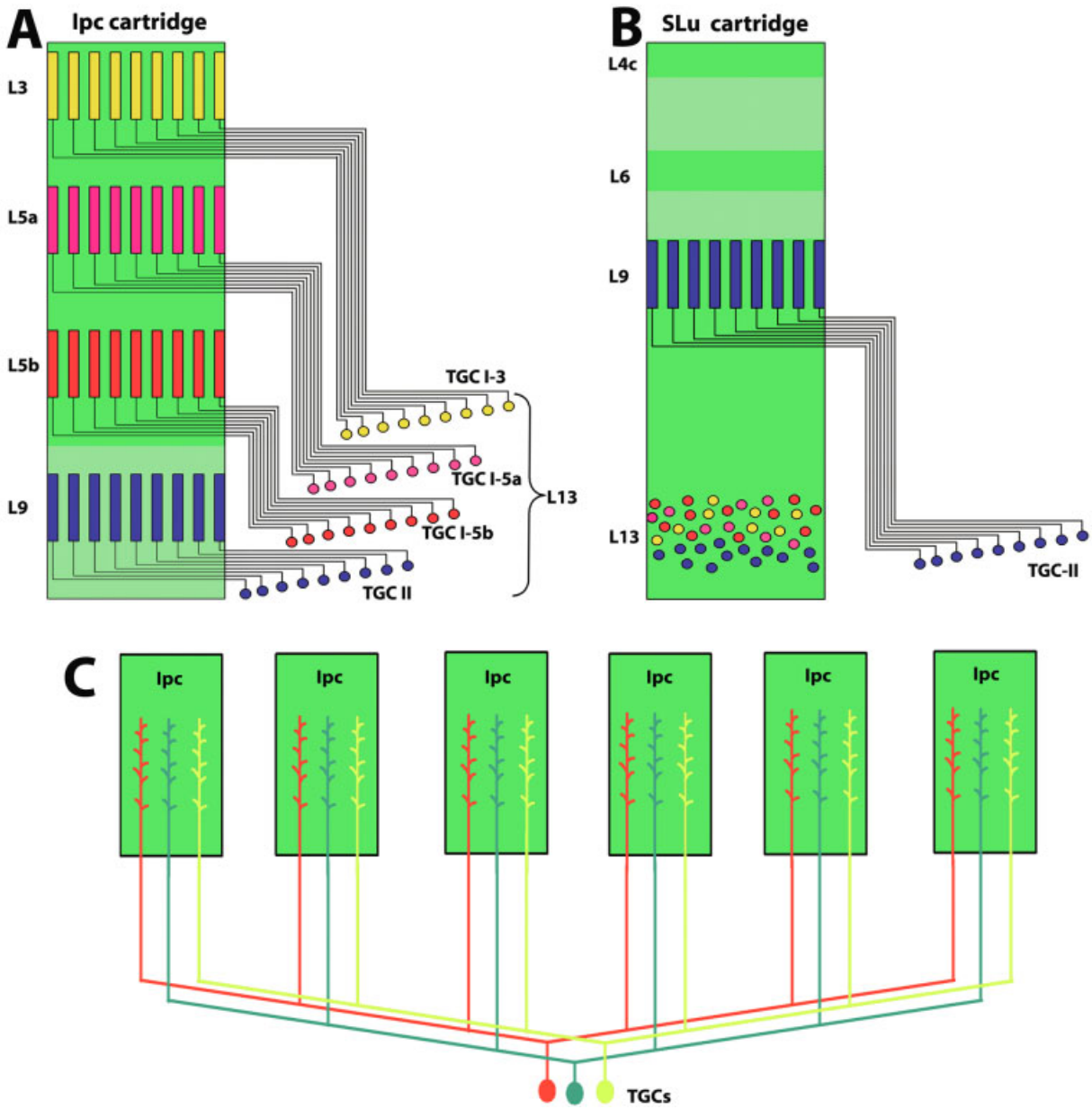

Fig. 20. Schematic drawings of the proposed cellular circuitry of Ipc and SLu axons terminating on bottlebrushes of type I and II TGCs. **A:** Individual Ipc endings (green) densely arborize in layers 3, 5a, and 5b and contact bottlebrushes of three subtypes of type I TGCs, TGC I-3 (yellow), TGC I-5a (pink), TGC I-5b (red), and probably type II TGCs (blue) to a lesser extent. In each of these layers one Ipc ending contacts numerous bottlebrushes from different TGCs of the same subtype, but only contacts a single bottlebrush from any individual TGC neuron. **B:** SLu endings (green) contact bottlebrushes of type II TGCs (blue) and probably the somata and proximal dendrites of all types of TGCs. Dark and light green indicate heavy and light inputs of Ipc/SLu in the TeO. **C:** Individual TGCs are innervated by numerous Ipc neurons with each of its bottlebrush contacting one Ipc ending.

5b is about 4–5 μm in diameter. Since the spacing between bottlebrush endings of single TGCs is usually much larger than 50 μm in chicks (Luksch et al., 1998), individual Ipc terminations are likely to terminate on only a single dendritic ending from an individual TGC neuron, but on numerous endings from different TGCs of the same subtype. The vertical distribution of a single brush-like ending then can act on spatially related TGCs of the remaining Type I TGC that receive input from the same point of the visual field, but from different ganglion cells.

SLu axons do not arborize in layer 3 and the major portion of layer 5; thus, their synaptic interaction with bottlebrushes of type I TGCs is rather restricted. On the contrary, SLu may contribute to the modulation of the TGCs by contacting the distal dendrites of type II TGCs in layer 9, and in contrast to the sparse innervation of layer 9 by Ipc (Fig. 20B). SLu terminations are 120–180 μm wide and may contact more than one bottlebrush of individual TGCs. In addition, the dense arborization of SLu in layers 10b–13 may contact the somata and primary den-

drites of both types of TGCs. The synaptic mechanism of these proposed connections remains unclear, as no distinct bouton-like structures were detected on SLu axons.

We propose that Ipc and SLu axons serve to produce precisely coordinated activation in the time domain across the various processing channels of type I and II TGCs within a single small region of the congruent receptive field of these cells. As a result, retinally evoked excitation at a given tectal locus will lead to a complex pattern of reafferent excitation and inhibition through all feedback loops of the isthmic complex. Given that distinct subtypes of TGCs project on functionally distinct subdivisions of the nucleus rotundus (Benowitz and Karten, 1976; Mpodozis et al., 1996; Karten et al., 1997; Luksch et al., 1998; Hellmann and Güntürkün, 2001; Marín et al., 2003), the isthmic circuitry provides an early stage of interaction across information-processing streams. In a general context, this circuitry might maintain spatial relatedness and thus overcome an inherent problem of splitting information into various processing streams.

Despite the present circumstantial evidence of substantial projections of the Ipc and SLu on the TGCs, we have no direct evidence as to the immediate postsynaptic targets of the Ipc or SLu. The presence of nicotinic AChR within the TGC somata (Britto et al., 1992) is suggestive of a major role for cholinergic inputs in the regulation of TGCs. However, the immunoreactivity for the nicotinic nAChR is mainly confined to the somata and proximal dendrites. This may reflect the relative insensitivity of immunohistochemistry in detecting low levels of immunoreactivity in very thin distal dendrites, or may indicate a selective distribution within the various domains of the TGCs. Whether TGCs express muscarinic receptors at their distal terminals remains unknown. Furthermore, our emphasis on the possible synapses of Ipc and SLu on the TGCs should not obscure isthmic inputs on other tectal systems.

Several lines of evidence in studies of the nucleus isthmi of fish and amphibians have led to the suggestion that the nucleus isthmi plays a role in depth perception and/or stereopsis (Gruberg and Udin, 1978; Collett et al., 1987; Wiggers, 1998). These studies identified the existence of a retinotopic projection of the nucleus isthmi on both the ipsilateral and contralateral TeO. A similar, although less substantial, projection has been identified in various mammalian brains (rats: Linden and Perry, 1983; cats: Graybiel, 1978; monkeys: Baizer et al., 1991). As discussed in our previous article (Wang et al., 2004) and confirmed in the current study, we found no evidence of any neurons in Ipc, SLu, or Imc that project on the opposite optic tectum in chicks. This is puzzling, as birds appear to have particular needs for accurate depth perception in flight and landing, and stereopsis may play a major role in the high speed motor acts required for feeding in insectivorous birds, fish-hunting birds such as herons, as well as the bifrontally directed eyes of owls. However, in the light of recent work on owls (Wagner and Frost, 1993; van der Willigen et al., 1998; Nieder and Wagner, 2001) and previous studies in pigeons (Perisic et al., 1971; Karten et al., 1973), the mechanisms that exploit binocular information in birds are likely to be contained in the visual wulst, the homolog to the striate cortex in mammals.

ACKNOWLEDGMENTS

We thank Kristin Maczko at Stanford University (California) for critical reading and comments on the article, Dr. J. Martin Wild at the University of Auckland (New Zealand) for valuable discussions, and Agnieszka Brzozowska-Prechtl at the University of California at San Diego for technical assistance.

LITERATURE CITED

Baizer JS, Whitney JF, Bender DB. 1991. Bilateral projections from the parabigeminal nucleus to the superior colliculus in monkeys. Exp Brain Res 86:467–470.

Baleydier C, Magnin M. 1979. Afferent and efferent connections of the parabigeminal nucleus in cat revealed by retrograde axonal transport of horseradish peroxidase. Brain Res 161:187–198.

Benowitz LI, Karten HJ. 1976. Organization of the tectofugal visual pathway in the pigeon: a retrograde transport study. J Comp Neurol 167: 503–520.

Brecha N. 1978. Some observations on the organization of the avian optic tectum: afferent nuclei and their tectal projections. PhD Thesis, State University of New York: Stony Brook.

Britto LR, Keyser KT, Lindstrom JM, Karten HJ. 1992. Immunohistochemical localization of nicotinic acetylcholine receptor subunits in the mesencephalon and diencephalon of the chick (*Gallus gallus*). J Comp Neurol 317:325–340.

Ciani F, Franceschini V. 1982. The pattern of acetylcholinesterase distribution in the normal and retino-deprived optic tectum of newt. Z Mikrosk Anat Forsch 96:600–612.

Ciani F, Contestabile A, Villani L. 1978. Acetylcholinesterase activity in the normal and retino-deprived optic tectum of the quail. Light and electron microscopic histochemistry and biochemical determination. Histochemistry 59:81–95.

Collett TS, Udin SB, Finch DJ. 1987. A possible mechanism for binocular depth judgments in anurans. Exp Brain Res 66:35–40.

Cowan WM, Cuénod M. 1975. The use of axonal transport for the study of neural connections: a retrospective survey. In: Cowan WM, Cuénod M, editors. The use of axonal transport for the study of neural connections. New York: Elsevier Scientific. p 1–24.

Diamond IT, Fitzpatrick D, Conley M. 1992. A projection from the parabigeminal nucleus to the pulvinar nucleus in Galago. J Comp Neurol 316:375–382.

Dudkin EA, Gruberg ER. 2003. Nucleus isthmi enhances calcium influx into optic nerve fiber terminals in *Rana pipiens*. Brain Res 969:44–52.

Dye JC, Karten HJ. 1996. An in vitro study of retinotectal transmission in the chick: role of glutamate and GABA in evoked field potentials. Vis Neurosci 13:747–758.

Edwards SB, Ginsburgh CL, Henkel CK, Stein BE. 1979. Sources of subcortical projections to the superior colliculus in the cat. J Comp Neurol 184:309–330.

Ericson J, Morton S, Kawakami A, Roelink H, Jessell TM. 1996. Two critical periods of Sonic Hedgehog signaling required for the specification of motor neuron identity. Cell 87:661–73.

Fedtsova NG, Turner EE. 1995. Brn-3.0 expression identifies early postmitotic CNS neurons and sensory neural precursors. Mech Dev 53:291–304.

Fedtsova N, Turner EE. 2001. Signals from the ventral midline and isthmus regulate the development of Brn3.0-expressing neurons in the midbrain. Mech Dev 105:129–144.

Felix D, Wang SR, Yan K, Wang YT. 1985. The effect of acetylcholine on neurones of the amphibian nucleus isthmi. Brain Res 326:313–316.

Gerrero MR, McEvilly RJ, Turner E, Lin CR, O'Connell S, Jenne KJ, Hobbs MV, Rosenfeld MG. 1993. Brn-3.0: a POU-domain protein expressed in the sensory, immune, and endocrine systems that functions on elements distinct from known octamer motifs. Proc Natl Acad Sci U S A 90:10841–10845.

Graybiel AM. 1978. A satellite system of the superior colliculus: the parabigeminal nucleus and its projections to the superficial collicular layers. Brain Res 145:365–374.

Gruberg ER, Udin SB. 1978. Topographic projections between the nucleus isthmi and the tectum of the frog *Rana pipiens*. J Comp Neurol 179: 487–500.

Gruberg ER, Wallace MT, Caine HS, Mote MI. 1991. Behavioral and

physiological consequences of unilateral ablation of the nucleus isthmi in the leopard frog. Brain Behav Evol 37:92–103.

Gruberg ER, Hughes TE, Karten HJ. 1994. Synaptic interrelationships between the optic tectum and the ipsilateral nucleus isthmi in *Rana pipiens*. J Comp Neurol 339:353–364.

Güntürkün O. 1987. A Golgi study of the isthmic nuclei in the pigeon (*Columba livia*). Cell Tissue Res 248:439–448.

Güntürkün O, Remy M. 1990. The topographical projection of the nucleus isthmi pars parvocellularis (Ipc) onto the tectum opticum in the pigeon. Neurosci Lett 111:18–22.

Hall WC, Fitzpatrick D, Klatt LL, Raczkowski D. 1989. Cholinergic innervation of the superior colliculus in the cat. J Comp Neurol 287:495–514.

Harting JK, Glendenning KK, Diamond IT, Hall WC. 1973. Evolution of the primate visual system: anterograde degeneration studies of the tecto-pulvinar system. Am J Phys Anthropol 38:383–392.

Hayes BP, Webster KE. 1975. An electron microscope study of the retinoreceptive layers of the pigeon optic tectum. J Comp Neurol 162:447–465.

Hellmann B, Güntürkün O. 2001. Structural organization of parallel information processing within the tectofugal visual system of the pigeon. J Comp Neurol 429:94–112.

Hellmann B, Manns M, Güntürkün O. 2001. Nucleus isthmi, pars semilunaris as a key component of the tectofugal visual system in pigeons. J Comp Neurol 436:153–166.

Horton JC. 1984. Cytochrome oxidase patches: a new cytoarchitectonic feature of monkey visual cortex. Philos Trans R Soc Lond B Biol Sci 304:199–253.

Hughes TE. 1990. A light- and electron-microscopic investigation of the optic tectum of the frog, Rana pipiens. I. The retinal axons. Vis Neurosci 4:499–518.

Hunt SP, Brecha N. 1984. The avian optic tectum: a synthesis of morphology and biochemistry. In: Vanegas H, editor. Comparative neurology of the optic tectum. New York: Plenum Press. p 619–648.

Hunt SP, Künzle H. 1976. Observations on the projections and intrinsic organization of the pigeon optic tectum: an autoradiographic study based on anterograde and retrograde, axonal and dendritic flow. J Comp Neurol 170:153–172.

Hunt SP, Streit P, Künzle H, Cuénod M. 1977. Characterization of the pigeon isthmo-tectal pathway by selective uptake and retrograde movement of radioactive compounds and by Golgi-like horseradish peroxidase labeling. Brain Res 129:197–212.

Jeon CJ, Spencer RF, Mize RR. 1993. Organization and synaptic connections of cholinergic fibers in the cat superior colliculus. J Comp Neurol 333:360–374.

Jiang ZD, King AJ, Moore DR. 1996. Topographic organization of projection from the parabigeminal nucleus to the superior colliculus in the ferret revealed with fluorescent latex microspheres. Brain Res 743: 217–232.

Johnson CD, Epstein ML. 1986. Monoclonal antibodies and polyvalent antiserum to chicken choline acetyltransferase. J Neurochem 46:968–976.

Karten HJ, Hodos W. 1967. A stereotaxic atlas of the brain of the pigeon (*Columba livia*). Baltimore: Johns Hopkins Press.

Karten HJ, Hodos W, Nauta WJ, Revzin AM. 1973. Neural connections of the "visual wulst" of the avian telencephalon. Experimental studies in the piegon (*Columba livia*) and owl (*Speotyto cunicularia*). J Comp Neurol 150:253–278.

Karten HJ, Cox K, Mpodozis J. 1997. Two distinct populations of tectal neurons have unique connections within the retinotectorotundal pathway of the pigeon (*Columba livia*). J Comp Neurol 387:449–465.

Katz DM, Karten HJ. 1983. Subnuclear organization of the dorsal motor nucleus of the vagus nerve in the pigeon, *Columba livia*. J Comp Neurol 217:31–46.

King WM, Schmidt JT. 1991. The long latency component of retinotectal transmission: enhancement by stimulation of nucleus isthmi or tectobulbar tract and block by nicotinic cholinergic antagonists. Neuroscience 40:701–712.

Kuenzel WJ, Masson M. 1988. A stereotaxic atlas of the brain of the chick (*Gallus domesticus*). Baltimore: Johns Hopkins University Press.

Le Gros Clark WE. 1933. The medial geniculate body and the nucleus isthmi. J Anat 67:536–548.

Linden R, Perry VH. 1983. Retrograde and anterograde-transneuronal degeneration in the parabigeminal nucleus following tectal lesions in developing rats. J Comp Neurol 218:270–281.

Lu Y, Monsivais P, Tempel BL, Rubel EW. 2004. Activity-dependent regulation of the potassium channel subunits Kv1.1 and Kv3.1. J Comp Neurol 470:93–106.

Luksch H. 2003. Cytoarchitecture of the avian optic tectum: neuronal substrate for cellular computation. Rev Neurosci 14:85–106.

Luksch H, Cox K, Karten HJ. 1998. Bottlebrush dendritic endings and large dendritic fields: motion-detecting neurons in the tectofugal pathway. J Comp Neurol 396:399–414.

Luksch H, Karten HJ, Kleinfeld D, Wessel R. 2001. Chattering and differential signal processing in identified motion-sensitive neurons of parallel visual pathways in the chick tectum. J Neurosci 21:6440–6446.

Major DE. 2003. The functional and evolutionary signification of cellular morphology in the mammalian optic tectum. PhD Thesis, University of California, San Diego, La Jolla, CA.

Major DE, Luksch H, Karten HJ. 2000. Bottlebrush dendritic endings and large dendritic fields: motion-detecting neurons in the mammalian tectum. J Comp Neurol 423:243–260.

Marín G, Letelier JC, Henny P, Sentis E, Farfán G, Fredes F, Pohl N, Karten HJ, Mpodozis J. 2003. Spatial organization of the pigeon tectorotundal pathway: an interdigitating topographic arrangement. J Comp Neurol 458:361–380.

Marín G, Mpdozis J, Sentis E, Ossandon T, Letelier JC. 2005. Oscillatory bursts in the optic tectum of birds represent re-entrant signals from the nucleus isthmi pars parvocellularis. J Neurosci 25:7081–7089.

Martínez S, Puelles L. 1989. Avian nucleus isthmi ventralis projects to the contralateral optic tectum. Brain Res 481:181–184.

Medina L, Reiner A. 1994. Distribution of choline acetyltransferase immunoreactivity in the pigeon brain. J Comp Neurol 342:497–537.

Méndez-Otero R, Rocha-Miranda CE, Perry VH. 1980. The organization of the parabigemino-tectal projections in the opossum. Brain Res 198: 183–189.

Mpodozis J, Cox K, Shimizu T, Bischof HJ, Woodson W, Karten HJ. 1996. GABAergic inputs to the nucleus rotundus (pulvinar inferior) of the pigeon (*Columba livia*). J Comp Neurol 374:204–222.

Mufson EJ, Martin TL, Mash DC, Wainer BH, Mesulam MM. 1986. Cholinergic projections from the parabigeminal nucleus (Ch8) to the superior colliculus in the mouse: a combined analysis of horseradish peroxidase transport and choline acetyltransferase immunohistochemistry. Brain Res 370:144–148.

Nieder A, Wagner H. 2000. Horizontal-disparity tuning of neurons in the visual forebrain of the behaving barn owl. J Neurophysiol 83:2967–2979.

Parameshwaran S, Carr CE, Perney TM. 2001. Expression of the Kv3.1 potassium channel in the avian auditory brainstem. J Neurosci 21:485–494.

Perisic M, Mihailovic J, Cuenod M. 1971. Electrophysiology of contralateral and ipsilateral visual projections to the Wulst in pigeon (*Columba livia*). Int J Neurosci 2:7–14.

Pfeiffer CP, Britto LR. 1997. Distribution of calcium-binding proteins in the chick visual system. Braz J Med Biol Res 30:1315–1318.

Ramón y Cajal S. 1899. Adiciones á nuestros trabajos sobre los centros ópticos de las aves. Micrográfica IV:77–86.

Ramón y Cajal S. 1911. Histology of the nervous system of man and vertebrates. Translated from Spanish to French by L. Azoulay, from the French to English by N. Swanson and L.W. Swanson (1995). New York, Oxford University Press.

Roldán M, Reinoso-Suarez F, Tortelly A. 1983. Parabigeminal projections to the superior colliculus in the cat. Brain Res 280:1–13.

Ross CD, Godfrey DA. 1985. Distributions of choline acetyltransferase and acetylcholinesterase activities in layers of rat superior colliculus. J Histochem Cytochem 33:631–641.

Sargent PB, Pike SH, Nadel DB, Lindstrom JM. 1989. Nicotinic acetylcholine receptor-like molecules in the retina, retinotectal pathway, and optic tectum of the frog. J Neurosci 9:565–573.

Scharrer E, Sinden J. 1949. A contribution to the chemoarchitectonics of the optic tectum of the brain of the pigeon. J Comp Neurol 91:331–336.

Schmidt JT. 1995. The modulatory cholinergic system in goldfish tectum may be necessary for retinotopic sharpening. Vis Neurosci 12:1093–1103. [Erratum: Vis Neurosci 13:597.]

Schmidt A, Roth G, Ernst M. 1989. Distribution of substance P-like, leucine-enkephalin-like, and bombesine-like immunoreactivity and acetylcholinesterase activity in the visual system of salamanders. J Comp Neurol 288:123–135.

Schoepfer R, Conroy WG, Whiting P, Gore M, Lindstrom J. 1990. Brain

alpha-bungarotoxin binding protein cDNAs and MAbs reveal subtypes of this branch of the ligand-gated ion channel gene superfamily. Neuron 5:35–48.

Sebestény T, Davies DC, Zayats N, Németh A, Tömböl T. 2002. The ramification and connections of retinal fibres in layer 7 of the domestic chick optic tectum: a Golgi impregnation, anterograde tracer and GABA-immunogold study. J Anat 200:169–183.

Sereno MI, Ulinski PS. 1987. Caudal topographic nucleus isthmi and the rostral nontopographic nucleus isthmi in the turtle, *Pseudemys scripta*. J Comp Neurol 261:319–346.

Sherk H. 1978. Visual response properties and visual field topography in the cat's parabigeminal nucleus. Brain Res 145:375–379.

Sherk H. 1979a. A comparison of visual-response properties in cat's parabigeminal nucleus and superior colliculus. J Neurophysiol 42:1640–1655.

Sherk H. 1979b. Connections and visual-field mapping in cat's tectoparabigeminal circuit. J Neurophysiol 42:1656–1668.

Sorenson EM, Parkinson D, Dahl JL, Chiappinelli VA. 1989. Immunohistochemical localization of choline acetyltransferase in the chicken mesencephalon. J Comp Neurol 281:641–657.

Streit P, Knecht E, Cuenod M. 1980. Transmitter-related retrograde labeling in the pigeon optic lobe: a high resolution autoradiographic study. Brain Res 187:59–67.

Titmus MJ, Tsai HJ, Lima R, Udin SB. 1999. Effects of choline and other nicotinic agonists on the tectum of juvenile and adult Xenopus frogs: a patch-clamp study. Neuroscience 91:753–769.

Tokunaga A, Otani K. 1978. Neuronal organization of the corpus parabigeminum in the rat. Exp Neurol 58:361–375.

Tömböl T, Németh A. 1998. GABA-immunohistological observations, at the electron-microscopical level, of the neurons of isthmi nuclei in chicken, *Gallus domesticus*. Cell Tissue Res 291:255–266.

Tömböl T, Egedi GY, Németh A. 1995. Some data on connections of neurons of nuclei isthmi of the chicken. J Hirnforsch 36:501–508.

Tömböl T, Eyre MD, Alpar A, Nemeth A. 2005. The axon arbourisation of nuclei isthmi neurons in the optic tectum of the chick and pigeon. A Golgi and anterograde tracer-study. Anat Embryol (Berl) [Epub ahead of print].

Udin SB, Fisher MD, Norden JJ. 1990. Ultrastructure of the crossed isthmotectal projection in Xenopus frogs. J Comp Neurol 292:246–254.

Vaage S. 1973. The histogenesis of the isthmic nuclei in chick embryos (Gallus domesticus). I. A morphological study. Z Anat Entwicklungsgesch 142:283–314.

van der Willigen RF, Frost BJ, Wagner H. 1998. Stereoscopic depth perception in the owl. Neuroreport 9:1233–1237.

Veenman CL, Reiner A, Honig MG. 1992. Biotinylated dextran amine as an anterograde tracer for single- and double-labeling studies. J Neurosci Methods 41:239–254.

Villani L, Contestabile A. 1982. Cytochemical study of cholinesterases in the normal and retino-derived optic tectum of reptiles. J Hirnforsch 23:55–66.

Wagner H, Frost BJ. 1993. Disparity sensitive cells in the owl have a characteristic disparity. Nature 364:796–798.

Wallace MT, Ricciuti AJ, Gruberg ER. 1990. Nucleus isthmi: its contribution to tectal acetylcholinesterase and choline acetyltransferase in the frog Rana pipiens. Neuroscience 35:627–636. [Erratum: Neuroscience 38:283.]

Wang SR. 2003. The nucleus isthmi and dual modulation of the receptive field of tectal neurons in non-mammals. Brain Res Brain Res Rev 41:13–25.

Wang YC, Frost BJ. 1991. Visual response characteristics of neurons in the nucleus isthmi magnocellularis and nucleus isthmi parvocellularis of pigeons. Exp Brain Res 87:624–633.

Wang SR (Wang SJ), Felix D, Frangi U. 1978. The role of glutamate in pigeon optic tectum. Brain Res 157:360–363.

Wang SR, Wang YC, Frost BJ. 1995. Magnocellular and parvocellular divisions of pigeon nucleus isthmi differentially modulate visual responses in the tectum. Exp Brain Res 104:376–384.

Wang LY, Gan L, Perney TM, Schwartz I, Kaczmarek LK. 1998. Contribution of the Kv 3.1 potassium channel to high-frequency firing in mouse auditory neurones. J Physiol 509:183–194.

Wang Y, Xiao J, Wang SR. 2000. Excitatory and inhibitory receptive fields of tectal cells are differentially modified by magnocellular and parvocellular divisions of the pigeon nucleus isthmi. J Comp Physiol A 186:505–511.

Wang Y, Major DE, Karten HJ. 2004. Morphology and connections of nucleus isthmi pars magnocellularis in chicks (*Gallus gallus*). J Comp Neurol 469:275–297.

Watanabe K, Kawana E. 1979. Efferent projections of the parabigeminal nucleus in rats: a horseradish peroxidase (HRP) study. Brain Res 168:1–11.

Whiting PJ, Liu R, Morley BJ, Lindstrom JM. 1987. Structurally different neuronal nicotinic acetylcholine receptor subtypes purified and characterized using monoclonal antibodies. J Neurosci 7:4005–4016.

Wiggers W. 1998. Isthmotectal connections in plethodontid salamanders. J Comp Neurol 395:261–272.

Woodson W, Reiner A, Anderson K, Karten HJ. 1991. Distribution, laminar location, and morphology of tectal neurons projecting to the isthmooptic nucleus and the nucleus isthmi, pars parvocellularis in the pigeon (*Columba livia*) and chick (*Gallus domesticus*): a retrograde labeling study. J Comp Neurol 305:470–488.

Wouterlood FG, Jorritsma-Byham B. 1993. The anterograde neuroanatomical tracer biotinylated dextran-amine: comparison with the tracer Phaseolus vulgaris-leucoagglutinin in preparations for electron microscopy. J Neurosci Methods 48:75–87.

Wu GY, Wang SR, Felix D. 1994. Effect of acetylcholine and NMDA on neurones of avian tectum and nucleus isthmi. Neuroreport 5:850–852.